applied sciences

MDPI

Review

Designing the Optimal Procedure: Role of CT Scan in the Planning of Transcatheter Structural Heart Interventions

Simone Circhetta [1], Edoardo Nobile [1], Aurelio De Filippis [1], Luisa Vicchio [1], Annunziata Nusca [1,*], Domenico De Stefano [2], Francesco Piccirillo [1], Valeria Cammalleri [1], Fabio Mangiacapra [1], Elisabetta Ricottini [1], Rosetta Melfi [1], Raffaele Rinaldi [1], Carlo Cosimo Quattrocchi [2], Francesco Grigioni [1] and Gian Paolo Ussia [1]

[1] Unit of Cardiac Sciences, Department of Medicine, Campus Bio-Medico University, 00128 Rome, Italy
[2] Unit of Diagnostic Imaging, Department of Medicine, Campus Bio-Medico University, 00128 Rome, Italy
* Correspondence: a.nusca@policlinicocampus.it

Abstract: Computed tomography (CT) scanning has recently assumed a first-pillar role in the preoperative planning of patients undergoing transcatheter structural heart procedures (e.g., transcatheter aortic valve implantation, TAVI; MitraClip; Triclip; left atrial appendage occlusion, LAAO). A careful preprocedural assessment is crucial for achieving the best possible result, and, currently, CT represents the paramount technique to obtain morphological data on cardiac and vessel structures, thus allowing to choose the most appropriate vascular approach, the type and size of devices, and all the required steps to meet procedural expectations. The image reconstruction accuracy also provides information to predict potential complications such as misplacements and leakages. This review aims to describe the role of CT in the decision-making approach of patients undergoing structural heart interventions and expand the clinicians' understanding of the benefits and drawbacks of this imaging technique.

Keywords: structural heart interventions; cardiac computed tomography; TAVI; MitraClip; Triclip; left appendage occlusion

check for updates

Citation: Circhetta, S.; Nobile, E.; De Filippis, A.; Vicchio, L.; Nusca, A.; De Stefano, D.; Piccirillo, F.; Cammalleri, V.; Mangiacapra, F.; Ricottini, E.; et al. Designing the Optimal Procedure: Role of CT Scan in the Planning of Transcatheter Structural Heart Interventions. *Appl. Sci.* **2023**, *13*, 1589. https://doi.org/10.3390/app13031589

Academic Editor: Julio Garcia Flores

Received: 10 December 2022
Revised: 19 January 2023
Accepted: 21 January 2023
Published: 26 January 2023

Copyright: © 2023 by the authors. Licensee MDPI, Basel, Switzerland. This article is an open access article distributed under the terms and conditions of the Creative Commons Attribution (CC BY) license (https://creativecommons.org/licenses/by/4.0/).

1. Introduction

In recent years, cardiac computed tomography (CT) has become a useful tool for morphological cardiac imaging and has complemented echocardiography for evaluating structural heart diseases [1]. Due to its high spatial resolution, CT provides relevant morphologic information concerning chamber size, myocardial mass, and vascular and valvular structures [2,3]. In this regard, CT can determine the presence of disease and estimate the significance of dysfunction. Furthermore, it allows the morphological evaluation of other organs, by scanning through different planes, identifying potential related diseases worthy to be considered [4–9]. For these reasons, CT has become crucial for the heart team to decide on the intervention's suitability, both surgical and, even more, percutaneous [10]. Furthermore, as demonstrated by our group, CT is very useful for a better assessment of valves' morphology in order to provide a proper preinterventional planning [11–13]. In transcatheter heart valvular interventions (THVI), CT is also capable of providing accurate measurements for vascular access and device choice, assisting with landing zone characterization, defining patient-specific risk, and potentially reducing cardiac and peripheral procedural complications [14]. Thus, this review aims to retrace the main fields of CT application in structural heart diseases and related transcatheter interventions by demonstrating that this kind of imaging technology has become a cornerstone for clinicians and interventional cardiologists in the decision-making approach and management of complications.

2. Computed Tomography and Aortic Valve

2.1. Anatomy of the Aortic Valve

The three sinuses of Valsalva, the aortic leaflets, or cusps and the three fibrous interleaflet triangles compose the aortic root, including the aortic valve. The first correspond to the luminal surface of the three bulges of the aortic root, which support their respective valvular leaflets. The right and left sinuses house the corresponding coronary arteries (right and left), while the third sinus does not. Because of this, the third sinus is usually described as the noncoronary sinus [15].

The leaflets include the free edge, the closing edge attached to the aortic root, the lunulae, the belly, and the leaflet attachments or hinges. The hinges of each cusp join with those of the other two at the level of the sinotubular junction and run in parallel for a short stretch, forming the three aortic valve commissures. On the other side, the three interleaflet triangles are formed, owing to the semilunar fashion of the aortic leaflets' attachment to the wall of the aortic root. Each triangle represents a triangular region between the attachments of two adjacent leaflets and sinuses of Valsalva. The superior attachment of aortic leaflets (thus, the acute angles of the interleaflet triangles) is represented by the sinotubular junction, which demarcates the aortic root from ascending aorta, whereas the inferior boundary is demarcated by the ventricular–aortic junction. In detail, the peripheral attachments of the three aortic leaflets join to create a "crown-like" annular ring. The crown's base is represented by a virtual ring formed by joining the inferior attachment points (nadir) of the leaflets within the left ventricle (Figure 1a,b). The semilunar hinges then cross another true ring, the anatomic ventricular–aortic junction [16].

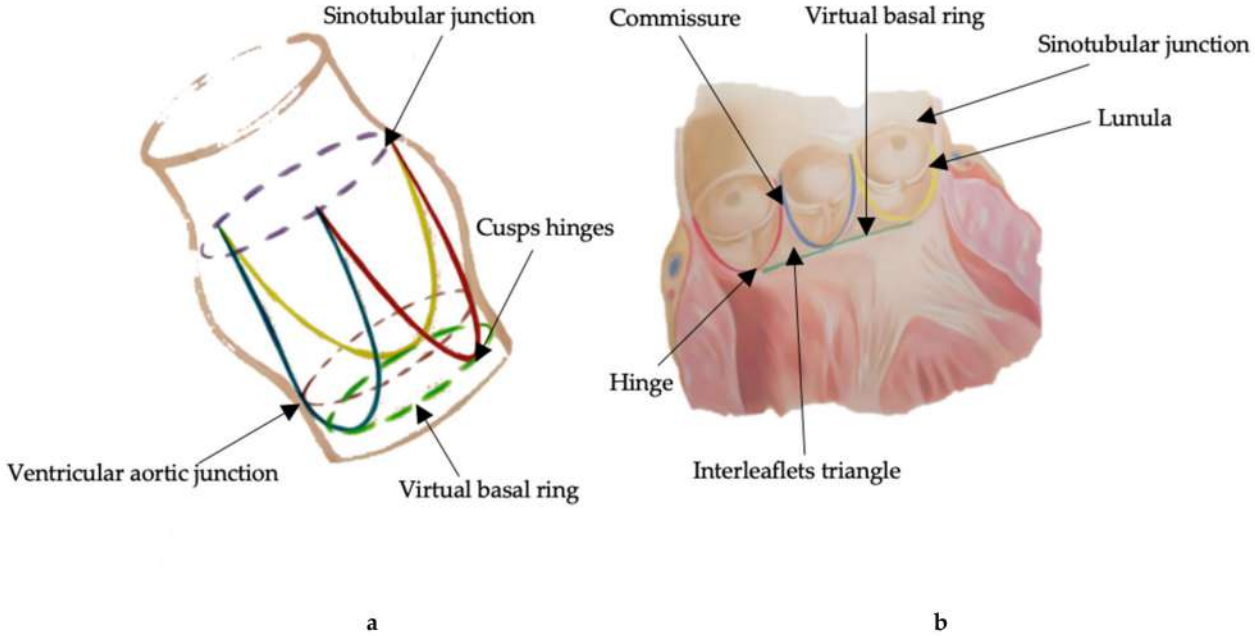

Figure 1. (**a**) Schematic representation of aortic valve anatomy. The dotted blue line indicates the sinotubular junction, the dotted green one depicts the virtual basal ring, and the dotted red one shows the ventricular aortic junction. (**b**) Graphic representation of an opened aortic root with its anatomical components.

2.2. Aortic Stenosis and TAVI (Transcatheter Aortic Valve Implantation) Indication

Aortic stenosis (AS) is the most prevalent valvular heart disease in Europe and the second most common in the United States. The progression of aortic stenosis depends on the severity of the condition at baseline [17]. Mean aortic valve gradients increased an average of 4, 6, and 10 mmHg/year in elderly patients with mild, moderate, and severe AS, respectively. Other factors that were associated with a faster hemodynamic progression included advanced aortic valve calcification, severe chronic renal failure, and anemia [18].

Without treatment, the average survival is only 2–3 years, with an increased risk of sudden death [18].

Transcatheter aortic valve implantation (TAVI) is a procedure that is now being recommended in older patients (≥75 years) or in those who are high risk (STSPROM/EuroSCORE II > 8%) or unsuitable for surgery. However, its indications are rapidly growing and progressively extending to younger patients with lower surgical risk [19]. Regarding aortic regurgitation, due to the difficult sealing and grasping of valves caused by the absence of calcium spots and the probable coexistence of dilated aortic root or ascending aorta, no clear recommendations exist, and the use of TAVI has been largely off-label [20–22].

2.3. CT Assessment of the Aortic Valve for Transcatheter Procedures

Multidetector computed tomography (MDCT) is considered crucial for the assessment of aortic valve defects (stenosis and regurgitation) and the preprocedural planning of TAVI [23].

On the technical side, TAVI CT assessment comprises two scans: an EKG-synchronized computed tomographic angiography (CTA) of the heart and aortic root, followed by a high-pitch non-EKG-synchronized CT multislice (CTM) for the evaluation of the access vessels. The two scans are combined into a complete protocol with a single contrast bolus through a peripheral vein. The amount of contrast medium should be calibrated to its concentration, patient's BMI, and kidney function (three thresholds should be considered: ≥60 mL/min/body surface area (BSA), 30–59 mL/min/BSA and <30 mL/min/BSA). Furthermore, for high-quality studies, according to the Cardiovascular Computed Tomography Society (SCCT), imaging should cover the entire cardiac cycle, and ALARA principles (as low as reasonably achievable) should be followed [24]. This means that the radiation dose that a patient could receive will vary depending on their weight or body mass index (BMI): 100 kV for patients with a BMI of 30 or less (or weight of 90 kg or less) to 120 kV for patients with a BMI of more than 30 kg (or weight more than 90 kg). Three scans are necessary to obtain useful parameters: the first is a basal one without contrast employed to calculate calcium scoring; a second one is used for cardiac evaluation with the administration of iodine contrast agent (after retrospective ECG synchronization); the last one should be extended from clavicles to the thigh's proximal portion in order to evaluate femoral and axillary accesses [24,25].

CT is almost universally accepted as a standard of care since its use has demonstrated a positive impact on clinical decision-making, favoring better post-TAVI clinical outcomes (Table 1) [26]. Therefore, Corcione et al. proposed a CT-based score called TAVI CT score, including the presence of nodular subvalvular calcium, the elliptical index (defined as the ratio of minimum aortic valve annulus diameter to maximum aortic valve annulus diameter), the aortic isthmus angle, the aorta ventricle angle, the presence of bicuspid valve, the coronary height, the detection of iliofemoral calcification, the access size, and the type of planned access, to predict outcomes. Notably, an increased risk of vascular complications was associated with higher scores [27]. Additionally, in a subanalysis of the WIN-TAVI registry, Spaziano et al. found that moderate or severe left ventricle outflow tract (LVOT) calcification detected by CT scan was an independent predictor of 1-year mortality or stroke [28]. The authors also reported that new pacemaker implantation (PMI) was independently associated with calcium volume of the right coronary cusp. In contrast, a protective effect on the same outcome was observed with the calcium volume of the noncoronary cusp. Lastly, according to this study, severe calcification of the noncoronary/right-coronary commissure can independently predict new atrial fibrillation onset [28]. In a study by Gama et al., it was demonstrated that membranous septum length measured at CT showed strong discriminatory ability for PMI [29]. Furthermore, Gegenava et al. highlighted that MDCT-derived global left ventricular longitudinal strain was a powerful predictor of all-cause mortality. As shown with the Kaplan–Meier curves, MDCT-derived LV GLS > −14% was related to higher cumulative rates of all-cause mortality than MDCT-derived LV GLS ≤ −14% [30]. In the following paragraphs, we discuss all specific

parameters obtained using CT that are considered of interest in the preprocedural planning for aortic valve replacement.

2.3.1. Peripheral Access

Femoral access is the preferred access for TAVI. MDCT imaging identifies patients with complex vasculature anatomies, which may impact the decision to use an alternative vascular approach (i.e., transapical, transaxillary, or direct aortic) [31]. Vessel size and diameters, degree of calcification, vessel tortuosity, and high-risk features can be properly identified by CT through multiple projections (Figure 2a,b).

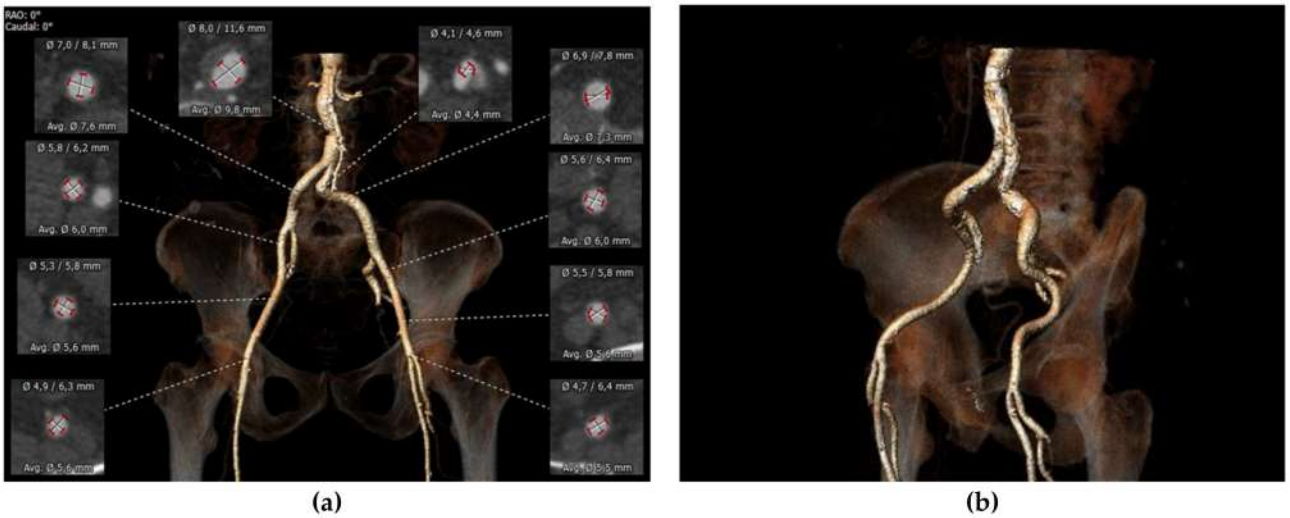

Figure 2. (**a**) Preoperative measurements of peripheral accesses for TAVI feasibility. (**b**) Preoperative femoral and iliac courses evaluation.

In a prospective study of 130 patients undergoing TAVI, Hayashida et al. found that vascular complications and 30-day mortality were associated with a sheath-to-femoral artery ratio (SFAR) of 1.05 or higher [32]. Later, Okuyama et al. proposed a change in this cut-off value, believing that this was too strict, providing high sensitivity but poor specificity, and 1.12 may be more appropriate (Table 1) [33].

Interestingly, the most recent valve delivery systems have a size ranging between 14 and 20 Fr, depending on the specific prosthesis valve type and size. While some years ago, a minimal lumen of femoral arteries of 6.0–6.5 mm was required, currently, with reduced delivery profiles, TAVI might also be indicated in patients with peripheral vessels as small as 5.0 mm [34].

2.3.2. Aortic Annulus

The aortic annulus for implanting percutaneous prostheses is not directly visible. It is a virtual ring that passes over a plane via the basal insertions (nadir) of the aortic valve cusps. It has an oval shape that varies during the cardiac cycle, even in patients with severe calcific AS. While the size of the aortic annulus was initially determined almost exclusively via two-dimensional transesophageal echocardiography (TEE), it has been proven that the aortic annulus is a dynamic measure during the cardiac cycle. Thus, 2D imaging could not be precise enough, and only 3D imaging can display a correct measurement. Furthermore, compared with a two-dimensional assessment of the annulus, MDCT-based measures have been proven to be highly reproducible and provide a deeper understanding of annular geometry [35]. Jurenkak et al. found that, during the cardiac cycle, the aortic root varies its shape, suggesting that an MDCT evaluation during the early systole phase is the best choice for TAVI planning [36].

Annular dimension can be quantified with multiple methods: cubic spline interpolation, polygon, attenuation/Hounsfield-unit-based contour detection, and freehand contour.

ECG-synchronized, ideally multiphasic, dataset should be used for proper measurement, identifying the reconstruction phase with the largest annular dimensions, thus ensuring accurate device sizing [24]. MDCT sizes the aortic annulus using annular area and perimeter measurements. In the Pivotal Trial of Medtronic Corevalve and the PARTNER 3 trial, it was demonstrated that annulus sizing based on CT measurements reduces the risk of complications such as paravalvular leakages. Moreover, the aortic annulus perimeter or cross-sectional area is superior to the annulus diameter for reducing the likelihood of paravalvular aortic regurgitation (PAR) [37,38] (Figure 3).

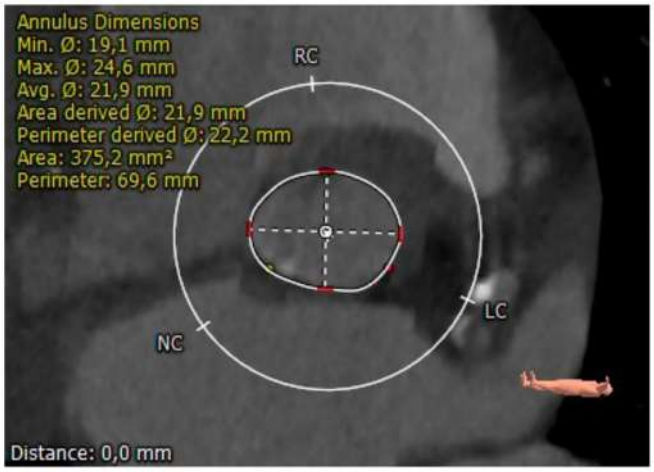

Figure 3. CT measurements of perimeter and area of aortic annulus.

Another goal of current CT sizing algorithms is to calculate a certain degree of oversizing of the transcatheter heart valve (THV) to avoid the post-implantation occurrence of paravalvular leaks (PVLs). It depends on the type of THV and the measurement used (perimeter/area). Self-expandable devices need more oversizing than balloon-expandable prostheses. Conversely, severe oversizing using balloon-expandable devices might increase the annular damage. Additionally, a 10 per cent perimeter oversize does not equal a 10 per cent area oversize, but it is closer to 20 per cent [39].

2.3.3. Aortic Leaflets

Three major parameters regarding aortic leaflets should be carefully considered during the preprocedural planning for TAVI: the number of cusps, the degree of leaflet calcification, and the height of the leaflets to the coronary ostia. MDCT has been proven to be superior to trans thoracic echocardiogram to discriminate aortic valvular morphology and the exact location and quantification of calcifications [40] (Figure 4a,b).

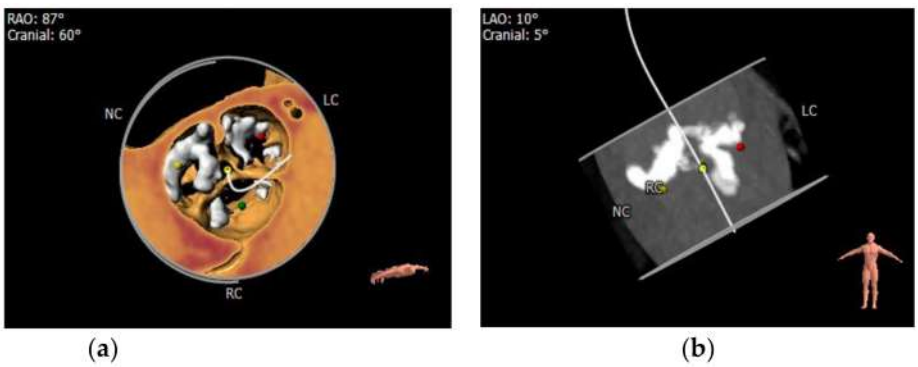

Figure 4. (**a**) Calcium degree and morphology evaluation of the aortic valve by CT. (**b**) LAO–cranial view for calcium location assessment.

The bicuspid aortic valve (BAV) is an important risk factor for premature aortic stenosis and challenging anatomy for percutaneous interventions. Thus, patients with bicuspid valves were excluded in the largest trials regarding TAVI due to complex anatomic features (i.e., more calcified, and asymmetrical leaflets, annular eccentricity, and associated aortic dilation). However, in recent years, the interest in this topic has rapidly grown, and the first data appear to be quite satisfactory [41]. BAV has historically been diagnosed with echocardiography that, compared with pathologic analyses obtained from cardiac surgery, can detect this kind of valve morphology in a range between 54 and 93%. Nevertheless, CT was found to be superior to transthoracic echocardiography, especially in patients with extensively calcified aortic valves [42] (Figure 5). In fact, taking into account echocardiographic and tomographic images of fifty patients with AS plus probable bicuspid aortic valve and comparing with surgical findings, Tanaka et al. found that CT data were not significantly different from the intraoperative ones, but the echocardiographic were [42].

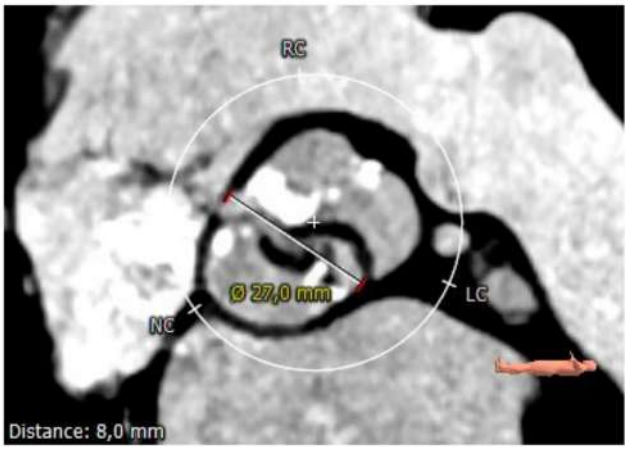

Figure 5. CT image of bicuspid valve.

MDCT images should assess several anatomical aspects in the setting of bicuspid aortic valves: the location of raphe by reviewing the commissures symmetry from the basal plane to the sinotubular junction, the specific morphology according to the Sievert classification, the extent of leaflet asymmetry, the degree of calcification, and the length and width of the raphe into the lumen. Indeed, more paravalvular regurgitation due to incomplete valve expansion could be associated with longer calcified raphe and calcium impingement > 4 mm [43].

Quantifying aortic valve calcification by noncontrast CT (CT-AVC) has demonstrated good accuracy in defining the valvular calcification burden (location, extent, and severity), demonstrating satisfactory concordance with echocardiography, and providing incremental prognostic information. CT-AVC has been reported to correlate significantly with peak velocity, mean gradient, and the aortic valvular area measured by echocardiography [44]. AVC is typically assessed by analyzing 1.5–3 mm slice thicknesses CT scans using prospective or retrospective electrocardiogram (ECG) gating and at lower tube current than contrast-enhanced CT studies, thus resulting in a low radiation dose of approximately 1 mSv. AVC can be measured by numerous methods, including Agatston, mass, and volumetric scores. Among these, the first method is more frequently employed.

Electron-beam and multidetector row CT studies demonstrate that the severity of AVC is a robust prognostic predictor in asymptomatic patients with severe AS (Table 1) [45]. Therefore, worse outcomes have been experienced by asymptomatic patients with severe AS and high calcium scores compared with those with low scores [46]. Moreover, preoperatively AVC assessment is crucial for TAVI because it has been demonstrated to negatively affect procedural success and outcomes given the greater presence of paravalvular regurgitation, conduction abnormalities, aortic annulus rupture, coronary ostia occlusion, and stroke. Furthermore, Leber et al. found that, in an analysis of 68 patients undergoing

TAVI, calcium score significantly correlated with 30-day major adverse cardiac events (MACE) and 1-year mortality and with the incidence and severity of post-procedural aortic regurgitation. Patients with calcium scores > 750 experienced a significantly lower 1-year survival rate than those with <750 [47]. Haensig et al. confirmed these findings in a series of 120 patients receiving an Edwards SAPIEN prosthesis via a transapical approach [48].

Extensive calcification of the aortic cusps also represents a risk factor for obstruction of the left main coronary artery during THV deployment [31]. Additionally, Lee et al. found that subjects with at least mild–moderate post-procedural aortic regurgitation had higher AVC scores than patients with no PAR on follow-up [49]. Unbehaun et al. evaluated the amount of calcifications of the aortic landing zone, including the left ventricle outflow tract (LVOT), aortic annulus, and valvular cusps in 307 patients undergoing transapical TAVI, using a semiquantitative (4-point scale) and quantitative (Agatston calcium score) CT method. They found that an increased risk of PAR was strongly related to each 100-unit increment of the Agatston calcium score. Furthermore, a higher risk of AR was reported in patients with asymmetric cusp calcification and severe calcification of the landing zone [50]. Interestingly, Feuchtner et al. recently showed that paravalvular AR increased with the protruding rather than the "adherent" calcifications of the aortic valve and root [51].

2.3.4. Coronary Ostia

MDCT is crucial to identify the distance from the annulus/leaflet hinge point to the left main and right coronary ostia and the length of the corresponding coronary cusp (Figure 6a,b). Multiplanar, three-dimensional techniques allow better visualization and assessment of these complex structures and their relationships. For this reason, CT represents the preprocedural imaging gold standard for the evaluation of the risk of coronary occlusion. Even if there is no threshold value contraindicating the procedure, an increased risk of coronary occlusion was reported in patients with a coronary ostial height from the annulus < 12 mm and a sinus of Valsalva mean diameter < 30 mm. To ensure reproducibility, the height of the coronary ostia perpendicular to the plane of the annulus should be measured with an electronic caliper from the plane of the ring to the bottom of the ostium. No recommendations exist as to whether these measurements should be performed in systole or diastole [24].

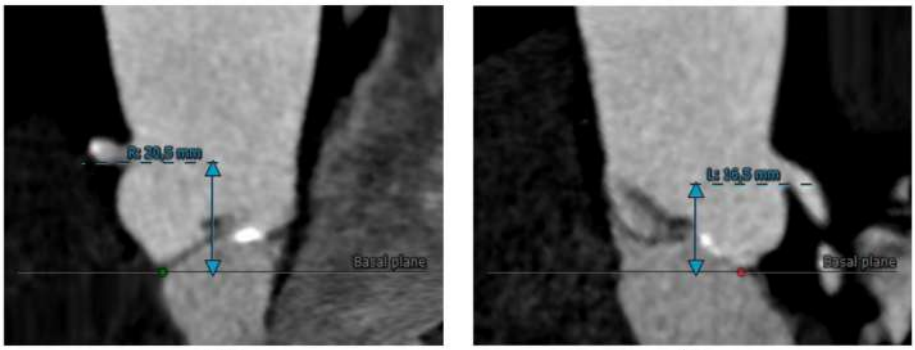

(**a**) (**b**)

Figure 6. (**a**) Right and (**b**) left coronary ostia height assessment by CT images.

Ribeiro et al. found that coronary occlusion most commonly affects the left coronary (88.6 per cent) and occurs more commonly in women and following balloon expandable TAVI. In a systematic review, several parameters were found to be possible predictors of procedural complications: a low-lying coronary ostium < 10 to 12 mm from the basal leaflet insertion to the coronary ostium as measured by MDCT, mean sinus of Valsalva diameter of <30 mm, and sinus of Valsalva diameter/annular diameter ratio of <1.25. Furthermore, according to this analysis, women appear to be more subjected to coronary occlusion because of smaller aortic root dimensions and lower coronary ostial height [52]. Probably, significantly oversized THV or aortic root dissection, the displacement of native bulky aortic

leaflets, impingement of the coronary ostia by the THV support structure, the embolization of calcium, thrombus, etc., are the mechanisms underlying coronary obstruction.

2.3.5. Sinotubular Junction (STJ) and Proximal Aorta

An inaccurate measure of the sinotubular junction and its degree of calcification may be associated with the incidence of prosthesis–patient mismatch (PPM) [53]. Small and severely calcified sinotubular junctions may also predispose to several complications: THV embolization, aortic root rupture during implantation of the THV, and balloon migration. In addition, using longer balloon-expandable valves, the sinotubular junction could be damaged with a transcatheter device.

The accuracy of MDCT imaging of the sinotubular junction depends on the measurement method. Compared with axial methods, double-oblique imaging yields similar findings to planimetry, and measurements obtained by double-oblique imaging are generally smaller, as was demonstrated in a study of patients with thoracic aortic aneurysms [54]. The height of the sinotubular junction should be measured perpendicular to the ring's plane using an electronic caliper from the annulus to its lowest point [24] (Figure 7a,b).

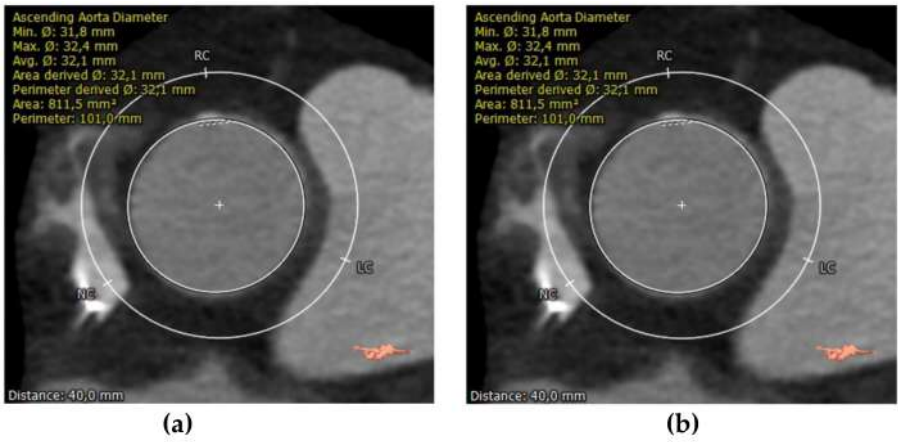

Figure 7. (**a**) Sinotubular junction and (**b**) proximal ascending aorta evaluated by CT for TAVI.

2.3.6. Left Ventricular Outflow Tract (LVOT) and Septum

Both self-expandable and balloon-expandable THVs extend their lower extremity into the left ventricular outflow tract (LVOT). A careful assessment of this region should be performed to minimize complications (Figure 8a,b).

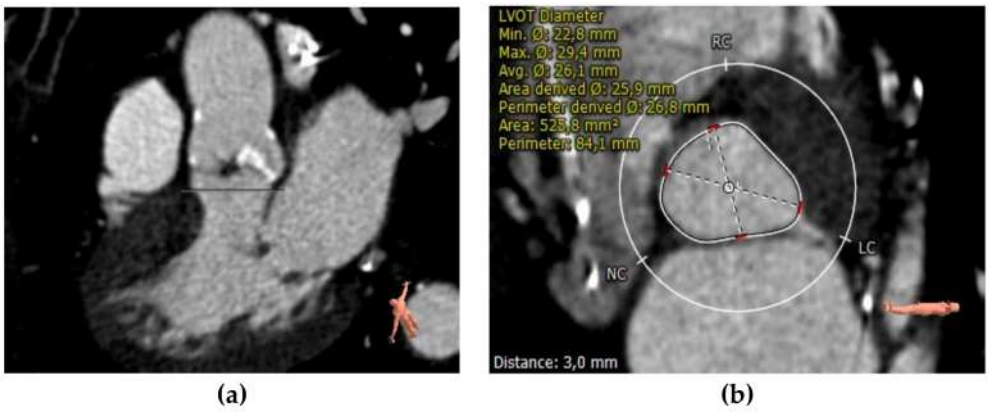

Figure 8. (**a**) LVOT calcium degree evaluation. (**b**) Preoperative LVOT measurements.

The proper seating of the THV and the risk of spontaneous repositioning after deployment can be affected by marked upper septal hypertrophy protruding in LVOT. Furthermore, prominent septal hypertrophy is associated with atrioventricular blocks and

the need for post-TAVI PMI [55]. Accordingly, Jilaihawi et al. showed that MDCT-based measurements of septal thickness predict the post-TAVI occurrence of AV blocks [56]. Septal hypertrophy causing significant LVOT obstruction is a contraindication to TAVI; however, as demonstrated by Moreno et al., proper modifications to THVs can allow successful implantation in this kind of patients [57]. Notably, Stolzmann et al. found that echocardiography tends to overestimate interventricular septum thickness compared with MDCT (up to 2.2 mm) [58] (Table 1).

Table 1. Main studies investigating the predictive role of CT-derived variables on related outcomes.

Study	CT-Derived Variable	Predicted Outcomes
Corcione et al. [27]	Valvular calcium score, elliptical index, aortic isthmus angle, aorta-ventricle angle, bicuspid valve, coronaries height, ilio-femoral calcifications, access size, type of planned access	Vascular complications
Spaziano et al. [28]	Left ventricle outflow tract calcium score	1-year mortality and stroke
Gama et al. [29]	Membranous septum length	Pacemaker implantation
Gegenava et al. [30]	Left ventricle global longitudinal strain	All-cause mortality
Hayashida et al. [32]	Sheath-to-femoral artery ratio > 1.05	Vascular complications and 30-day mortality
Okuyama et al. [33]	Sheath-to-femoral artery ratio > 1.12	Vascular complications and 30-day mortality
Rosenhek et al. [46]	Aortic calcium score	Paravalvular regurgitation, conduction abnormalities, aortic annulus rupture, coronary ostia occlusion and stroke
Leber et al. [47]	Aortic calcium score	30-day major adverse cardiac events, 1-year mortality and post-procedural aortic regurgitation
Haensig et al. [48]	Aortic calcium score	30-day major adverse cardiac events, 1-year mortality and post-procedural aortic regurgitation
Lee et al. [49]	Aortic calcium score	Para-aortic regurgitation
Unbehaun et al. [50]	Aortic calcium score	Para aortic regurgitation
Ribeiro et al. [52]	Low coronary ostium <10 to 12 mm, mean sinus of Valsalva diameter < 30 mm, sinus of Valsalva diameter/annular diameter ratio < 1.25	Coronary occlusion
Jilahawi et al. [56]	Septal thickness	Atrioventricular blocks

Furthermore, the risk of significative residual aortic regurgitation and second valve implantation can be affected by moderate or severe LVOT calcification. In this regard, Okuno et al. proposed a specific classification based on the severity of LVOT calcification: mild was detected in the presence of one nodule extending <5 mm in any dimension and covering <10% of the perimeter of the LVOT; moderate was documented in the presence of two nodules or one extending >5 mm in any direction or covering >10% of the perimeter of the LVOT; and severe was considered in the case of multiple nodules of single focus

extending >10 mm in length or covering >20% of the perimeter of the LVOT. Additionally, patients with moderate or severe LVOT calcification and treated with earlier-generation THVs suffered from an increased risk of annular rupture. The difference was not statistically significant among patients treated with newer generation prosthetic valves. Concordantly, it was observed that patients with moderate or severe LVOT calcification have an increased risk of death for all-cause mortality at one year [59].

3. Computed Tomography and Mitral Valve

3.1. Anatomy of the Mitral Valve

The mitral valve (MV) apparatus is composed of different parts: valvular annulus, two leaflets, chordae tendineae, and papillary muscles (Figure 9a,b).

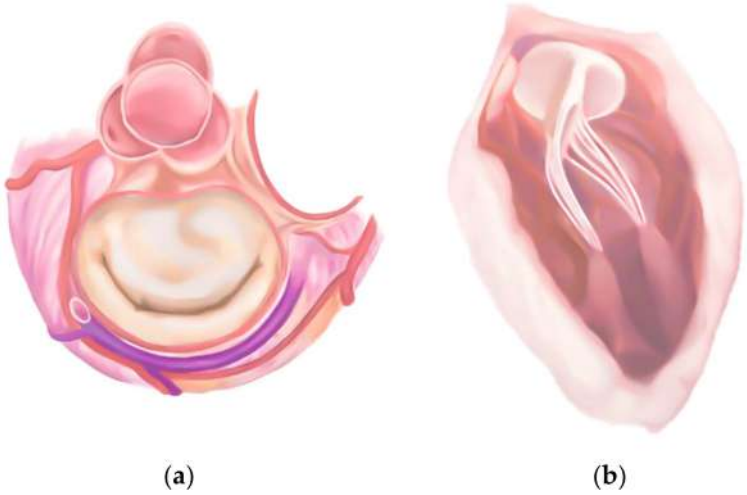

Figure 9. (**a**) Transverse and (**b**) sagittal planes of the mitral valve.

The MV annulus has a saddle shape. Its anterior flat portion, thus, the superior "horn", is connected by collagen fibers with the aortic annulus at the level of the noncoronary and the left aortic valve cusps. This fibrous part is called the aortomitral junction [60]. The posterior part of the mitral annulus includes the low saddle points in proximity to the lateral and medial commissures and the posterior saddle horn. This posterior part of the annulus is in continuity with the flexible, less fibrotic endocardium and may be subject to dilation. For this reason, it follows the myocardial contraction and relaxation, accentuating saddle height and decreasing circumferential area [61]. Notably, the MV annulus is surrounded by critical vascular structures, particularly by the coronary sinus (CS) posteriorly and the left circumflex artery laterally.

The anterolateral and posteromedial commissures separate the anterior and the posterior MV leaflets. The two MV leaflets are significantly different in size. The anterior leaflet, during systole, configures the posterior part of the left ventricular outflow tract, occupies one-third of the annulus, and is longer than the posterior leaflet, which sticks to two-thirds of the annulus. The posterior leaflet typically has two indentations which divide it into three individual scallops: a P1 lateral scallop (adjacent to the left atrial appendage), a larger central P2, and a medial P3 scallop according to Carpentier's classification. Contrarywise, the anterior leaflet is not anatomically divided into scallops, but its segments are referred to as A1, A2, and A3, corresponding to P1–3 [60].

The subvalvular apparatus of the MV includes chordae tendineae and papillary muscles. The primary cords anchor to the free edges of the leaflets, the secondary ones to the ventricular surface of the leaflets, and the tertiary ones originate from the left ventricular wall or muscle trabeculae at the posterior leaflet of the VM. Their function is to maintain, during systole, both leaflets in a position that allows their coaptation in systole without protrusion into the left atrium [62,63]. As far as the papillary muscles are concerned, the

anterolateral muscle arises from the apical-lateral third of the left ventricle. In contrast, the posteromedial muscle derives from the middle of the lower wall of the left ventricle. From their apex, the papillary cords take origin [64]. Their vascularization is important to understand some complications of infarction: notably, the left anterior descending and diagonal or marginal coronary branches feed the anterolateral papillary muscle; instead, in most cases, only one coronary artery (depending on the dominance, circumflex or right coronary artery) feeds the posteromedial papillary muscle. The different vascularization allows us to understand the susceptibility of the latter to ischemia and rupture.

3.2. Mitral Regurgitation and Transcatheter Interventions

Mitral regurgitation (MR) is the most common valvular pathological condition in the Western world [65]. It can be classified as primary or secondary. Therefore, a primary valve defect such as a flail or prolapse causes a primary MR. Secondary MR is due to the incomplete coaptation of the valve leaflets caused by the malposition of the subvalvular apparatus; it can be both ischemic and not [66].

Today, surgery remains the standard gold treatment for symptomatic MR patients. However, in recent years, transcatheter mitral valve surgery (TMVI) has emerged as a safe option for patients with high surgical risk [67]. According to the latest ESC 2021 guidelines on valvulopathies, transcatheter mitral valve repair can be considered in patients with chronic mitral regurgitation, symptomatic, with high surgical risk or inoperable, carefully avoiding futile treatments (IIA for secondary mitral regurgitation and IIB for primary mitral regurgitation) [19].

Recently, various techniques for the transcatheter mitral valve have been devised, often with reference to pre-existing surgical techniques. The MitraClip NT® System (Abbott Vascular, Santa Clara, CA, USA) is a repair system that conceptually emulates the "edge-to-edge" repair described by Maisano et al. [68]. It consists of a clip that hooks the two mitral leaflets simultaneously, reducing the width of the regurgitant orifice. Several randomized trials demonstrated the benefit of MitraClip in reducing mortality and hospitalization rate in patients with primary and functional MR [69–71]. Some other devices have been designed for the percutaneous treatment of MR, such as the Cardioband System® (Valtech Cardio, Or Yehuda, Israel) and the CARILLON Mitral Contour System® (Cardiac Dimensions, Inc., Kirkland, WA, USA), which mimic annuloplasty procedures. Unlike the MitraClip system, the latter technique can only be used for secondary etiology [72]. Finally, great interest revolves around transcatheter mitral valve replacement (TMVR); however, the growth of this technique, due to the complex anatomy of the mitral valve apparatus, the heterogeneity of pathology, and mitral annular dynamism, is undoubtedly slower than the explosive development of TAVI. As anticipated, several devices have been developed for this purpose, each with a different valve-anchoring mechanism (e.g., native flap engagement, mitral annulus clamping, apical tether, mitral annulus clamping, radial force, outer anchorage, flaps annular, subannular mitral annulus).

3.3. CT Assessment of the Mitral Apparatus for Transcatheter Procedures

Imaging modalities are necessary to provide information on mitral valve anatomy complexity and obtain a detailed plan for transcatheter procedures. Although echocardiography has represented the gold standard for pre- and post-treatment grading, diagnosis, and monitoring, MDCT has become widespread for interventional planning in patients who are candidates for TMVI. It allows rapid image acquisition time and wide availability, excellent spatial resolution, allowing high-quality 2D and 3D reconstructions of the entire mitral apparatus at any moment of the cardiac cycle, high reproducibility and relative operator independence, visualization, quantification of calcifications, and a complete view of the heart in its entirety and the chest wall [72]. CT provides relevant information on mitral leaflet pathology. Compared with echocardiography, CT provided the highest accuracy in identifying prolapse (sensitivity of 96%; specificity of 93%) [73].

Furthermore, cardiac CT is an excellent technique for diagnosing annular disjunction, a remodeling process associated with mitral valve prolapse, since observation of the entire cardiac cycle allows us to evaluate not only the degree of disjunction but also the dynamics of the ring [74]. In the context of secondary or functional MR, CT also provides essential information regarding the geometry of the valve and the remodeling process (including flap tenting heights and coaptation depth). Knowing that these data are essential for docking the device, CT provides details on the anatomy of the left ventricle, which is also crucial in assessing feasibility. A ventricular diameter greater than 70 mm is often considered an exclusion criterion for transcatheter procedures [75].

Exact measurements of the mitral annulus are critical for choosing the correct device size and, consequently, for an effective TMVI procedure [76]. Equally important is the understanding of the modifications of the annulus during the various phases of the cardiac cycle (modifications that vary according to the type of etiology of the insufficiency); based on this, the landing zone and the type of device are decided [77]. It appears evident that the annulus is larger in patients with mitral regurgitation than in controls, with a greater remodeling in an anterior–posterior, rather than lateral, direction [76]. Furthermore, in functional MR, the annulus reduces movement compared to primary MR [78]. According to Palmisano et al., some annular geometry changes in patients with severe mitral regurgitation were detected using CT. They demonstrated that the mitral valve annulus was larger in patients with severe MR, especially in patients with prolapse (Carpentier type II). It is curious how, in these patients, the largest dimensions were found in the systolic phase, unlike controls in which the largest area is found in the early diastolic phase [79].

3.3.1. Annulus Sizing

Measurement of the mitral annulus is of primary importance since inaccurate sizing has devastating consequences. Moreover, given the complex mitral annulus 3D shape, collecting annular sizing could be challenging [80]. A direct calculation method involves tracing the edges of the annulus on conventional two-, three-, four-chamber, and short-axis views along the posterior mitral leaflet insertion and fibrous continuity. However, this method is time-consuming and can lead to an oversized device, increasing the risk of left ventricular outflow tract obstruction (LVOT). Blanke et al. developed a more straightforward method that assumes assimilating the mitral annulus to a planar D shape; given these premises, the two fibrous trigones are connected along a virtually straight line, effectively excluding the anterior horn [81]. Since the dimensions of the mitral annulus change during the cardiac cycle, the calculations are performed in the cardiac cycle phase in which the annulus is larger. Area and perimeter are the most used measures. However, other parameters are developed, such as the trigone–trigone distance; the intercommissural distance, which corresponds to the maximum diameter of the annulus parallel to the trigone–trigone distance; the septum-lateral distance, which corresponds to the maximum diameter of the annulus perpendicular to the IC. It must be emphasized that each device refers to different parameters for sizing [79].

3.3.2. Predicting LVOT Obstruction

The LVOT lies between the mitro-aortic continuity and the interventricular septum. The placement of a transcatheter mitral valve prosthesis could extend and narrow the LVOT (neo-LVOT) due to anterior deflection of the AML [82]. Indeed, LVOT obstruction is a significant cause of mortality and morbidity following TMV replacement procedures (TMVR) [83]. CT can predict the size of anticipated neo-LVOT, thus predicting potential obstruction. A recent study demonstrated that a CT neo-LVOT area measuring 1.7 cm^2 or smaller predicts LVOT obstruction with a sensitivity of 96% and a specificity of 92% [84]. Notably, the neo-LVOT size is also dynamic; for this reason, it is usually measured throughout systole.

Notably, LVOT changes the cardiac cycle; therefore, this measurement is made in systole. Several device- and patient-specific factors could influence the size of the neo-

LVOT. The former include stent protrusion, flare, and skirt size [85]. A more ventricular position of the mitral prosthesis, defined as a ventriculo-atrial offset of 80:20 (i.e., 80% of the device is positioned on the ventricular side and the remaining 20% on the atrial side), increases the risk of neo-LVOT obstruction. On the other hand, patient-specific characteristics include aortomitral angle, basal septal thickness, and anterior mitral leaflet length. The aortomitral angle is defined as the internal angle between the central axis of the mitral and aortic annulus; in particular, the risk of obstruction increases when the measurement of this angle approaches or exceeds 90°. Another factor influencing the risk of obstruction is the thickness of the interventricular septum, particularly a value greater than 14 mm [86]. Finally, longer anterior leaflet lengths (>30 mm) are associated with the possibility of neo-LVOT obstruction [87]. All these parameters should be carefully evaluated before proceeding with percutaneous mitral valve replacement to reduce complications and improve procedure success.

3.3.3. Landing Zone

CT provides information about the potential landing zone, defined as the site where the mitral prosthetic device should be deployed. It varies according to the device used and the specific mitral defect (functional MRI or mitral prolapse). As mentioned, a landing zone of 80/20 should be achieved. This means that, after deployment, about 80% of the device should be located on the ventricular side, whereas the remaining 20% on the atrial side. However, many factors may affect landing zone definition, such as the presence of mitral annulus (MAC) calcification, annular disjunction, and atrioventricular platform (abnormal atrial displacement of the mitral valve leaflet hinge point). In those devices that are anchored by friction and radial force, the MAC in the landing zone is essential [80]. Hence, CT accurately estimates gravity, density, and magnitude. Furthermore, an atrioventricular shelf of the LV myocardium can often be found near the junction point of the posterior mitral leaflet in patients with basal myocardial remodeling [88]. The presence of this shelf is more relevant for those mitral devices that use the inferolateral basal myocardium for anchoring. Finally, in these patients, the measurements must be performed in the physiological position [80].

3.3.4. Mitral Anulus Calcification

MAC is crucial when considering TMVI; it has been demonstrated to be an independent predictor of an elevated mean diastolic gradient after the MitraClip procedure [89]. It also contraindicates the use of some valve replacement devices. CT is the gold standard for its diagnosis and characterization, demonstrating a higher diagnostic performance than MRI and echocardiography. Degenerative annular mitral calcification (MAC) is a common finding in the elderly, with an incidence of about 6% [87]. It is the consequence of a progressive calcification of the fibrous part of the mitral annulus. Although typically confined to the posterior border of the annulus, its extension may circumferentially involve the annulus. Another cause of MAC is caseous calcification of the mitral annulus (CCMA). CCMA has a different territory of distribution (typically the area close to the posterior mitral leaflet) and a different composition (with calcium disposition only in the periphery and a central zone of variable attenuation without contrast enhancement). Therefore, CT can accurately describe these formations and the exact distinction between MAC and CCMA [90].

3.3.5. Vascular Structures

Preprocedural planning for TMVI includes careful evaluation of surrounding vascular structures using CT. Therefore, a fundamental part of the evaluation concerns the course and patency of the circumflex artery (Cx) due to its proximity to the posterior mitral annulus. When this distance is too short, some transcatheter procedures are contraindicated due to the risk of vessel closure during the fixation of the device. The distance between these two structures should be measured on multiple views to avoid the risk of dissection, closure, or perforation of the coronary sinus (CS) during or after the procedure [91,92]. In particular,

the relationship between the distance and angle between these two structures and the procedural success of patients undergoing transcatheter annuloplasty with the Carillon device has been demonstrated [93]. Consistently, a distance of CS to Cx of <8.6 mm in the distal device landing zone has been shown to be predictive of complications on the circumflex artery [94].

3.4. Other Potential Use of CT in Transcatheter Mitral Valve Interventions

Choosing the optimal approach for TVMI is also essential in procedural planning, and CT plays a crucial role in this context. Thus, in patients undergoing a transapical procedure, CT can be used to understand which intercostal space is close to the apex of the left ventricle and could allow the device to be deployed perpendicular to the mitral annulus, thus avoiding obstruction, perivalvular leaks, and canting [80]. Although most mitral procedures require intraprocedural transesophageal echocardiography guidance, CT can determine the optimal site for the septal puncture in those with the transseptal approach. Although there are no specific guidelines, it is preferred to puncture the inferoposterior section to obtain good coaxiality to the mitral annulus [95]. Moreover, it is very useful to calculate the distance from the puncture site to the mitral valve.

CT is also helpful in determining the optimal fluoroscopic viewing angle of the mitral annulus for device deployment, which should be perpendicular to the mitral annulus (coplanar angle) [80]. Knowledge of this angle is fundamental for interventionists for accurate coaxial device positioning. Indeed, any change from this fluoroscopic angle can translate into inaccurate deployment, potentially increasing procedural complications.

In patients undergoing mitral valve-in-valve (VIV), CT can identify patients at higher risk of complications, providing information on the pre-existing prosthesis and thus predicting the risk of LVOT obstruction [90].

Finally, CT has a role in the follow-up of patients undergoing TMVI, especially in assessing the presence of any subclinical thrombosis. Although the clinical significance of the latter is not yet known, CT can diagnose this complication by highlighting it as a thickening of the hypodense flap with the decreased movement of the prosthetic flaps [96]. CT also has a role in predicting the risk of mitral stenosis after the MitraClip procedure. In a study by Kaewkes et al., annulus diameters (both anteroposterior and medial–lateral), annulus area, and mitral valve orifice area were inversely associated with transvalvular gradients [97].

4. Computed Tomography and Tricuspid Valve

4.1. Anatomy of the Tricuspid Valve

The tricuspid valve (TV) is the heart's largest and most anterior valve, with a mean orifice area of 8 cm^2 [98]. Its functional anatomy comprises four main parts: annulus, leaflets, chords, and papillary muscles (Figure 10).

Figure 10. Graphic representation of tricuspid valve anatomy.

Even upon surgical inspection, the annulus is slim and difficult to identify; it has a nonplanar D shape and forms a 45-degree angle to the sagittal plane. Moreover, its structure changes during the various phases of the cardiac cycle, reaching an increase of 30% during the early phase of diastole [99]. The leaflets broadly vary among individuals. Three flaps (anterior, medial, and septal) are distinguishable in 54% of cases, but four or more flaps are often present. The anterior leaflet is the most extensive and mobile, while the posterior is the shortest in the circumferential plane. The septal leaflet is the shortest in the radial plane and the least mobile [100]. The tendinous cords are redundant, ranging from 17 to 36 [101]. Accessorial cords arise from the right ventricular free wall. The chordal insertion in the TV is variable and consists of rough zone chords, free edge chords, deep chords, basal chords (the most common type), and fan-shaped chords (which are attached mainly to the commissures) [11]. The cords emerging from the anterior papillary muscle attach to the anterior and posterior leaflets. In contrast, from the posterior papillary muscle, which can be bifid, the cords depart for the posterior and septal leaflets. The septal papillary muscle, usually smaller than the previous ones, instead supplies the cords for the anterior and septal leaflets [101]. Other anatomical structures are fundamental in all procedures performed on TV and in the right ventricle (RV). The noncoronary aortic valve cusp, the atrioventricular nodule, and the bundle of cords are in proximity to the anteroseptal commissure. Moreover, the coronary sinus is anatomically close to the posterior septal commissure, while the right coronary artery is close to the TV annulus [98,102].

4.2. Tricuspid Regurgitation and Transcatheter Interventions

Tricuspid valve disease has consistently been underestimated. However, in recent years there has been important progress in percutaneous repair techniques, which has shifted the focus to this pathology. An important study in Olmsted County reported an age- and sex-adjusted prevalence of 0.55% of greater or equal to moderate tricuspid regurgitation (TR), mostly women [102]. The mortality of those patients was significantly higher than that of the matched cases with trivial TR [102]. Similar findings were reported by another large cohort study, where long-term, higher functional TR severity was associated with considerably worse survival independently of baseline characteristics [103]. The development and successful results of transcatheter aortic valve implantation, followed by transcatheter therapies for mitral valve disease, have also opened many opportunities for transcatheter treatment of TR [104]. For this reason, the need to develop adequate imaging techniques for preoperative planning in this type of procedure has become increasingly urgent.

4.3. CT Assessment of the Tricuspid Apparatus for Transcatheter Procedures

The multiphasic, contrast-enhanced, retrospective cardiac-gated CT acquisition enables multiplanar reconstruction of the entire heart silhouette, including the proximal main vessels, allowing a comprehensive understanding of the right heart anatomy (Figure 11) [105].

The amounts of contrast and radiation required have been considerably reduced with the new CT scanners, as well as the duration of the acquisition phase. It is also possible to perform more precise reconstructions even in elevated heart rates, such as atrial fibrillation, a widespread pathology in patients with significant TR [106]. Notably, a dedicated protocol for tricuspid valve CT acquisition is necessary; it requires opacification of the right heart cavities by a monophasic or biphasic injection with a mixture of saline and contrast in different percentages and following bolus tracking in the right ventricle or the pulmonary artery [107].

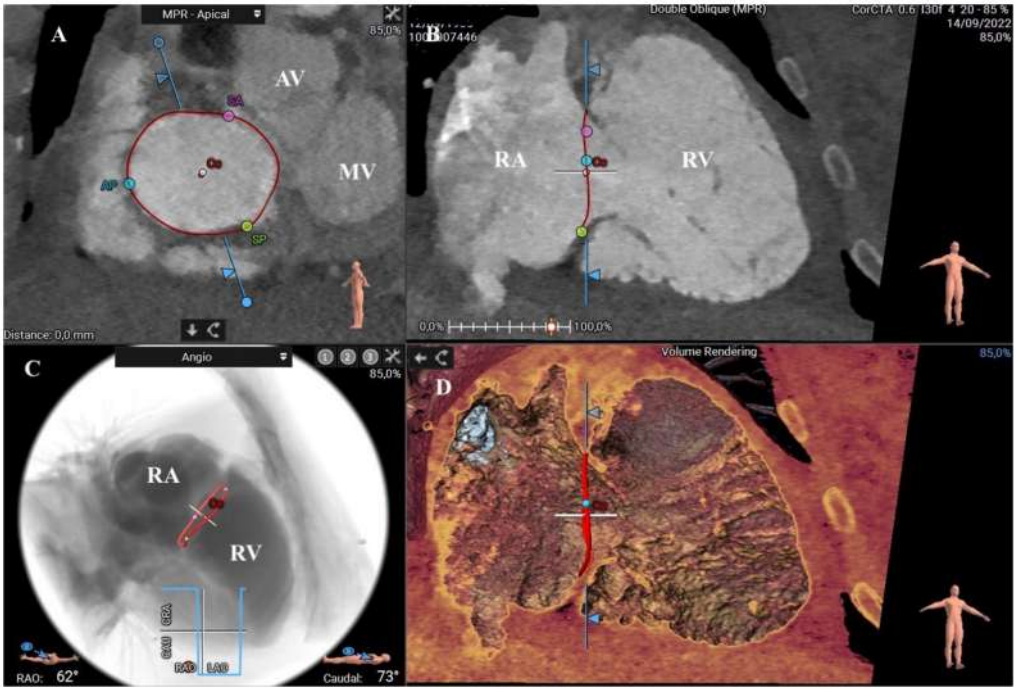

Figure 11. CT assessment of the tricuspid annulus using a semiautomated software-based approach (3mensio Structural Heart; Pie Medical Imaging, Maastricht, The Netherlands): (**A**) Transverse plane (short-axis) at level of tricuspid annulus that is delineated by the red line. The centroid of the tricuspid valve (Ce) and the three main commissures (SA: septal anterior, SP: septal posterior, AP: anteroposterior) are identified according to specific anatomical landmarks. (**B**) Coronal plane (long axis) at level of the anteroposterior diameter of the tricuspid annulus. (**C**) Fluoroscopic and angiographic simulation showing the three-dimensional position of the tricuspid annulus and commissures within the right heart chambers. (**D**) Three-dimensional recontraction by the volume rendering of the right chambers showing the geometrical spatial relationship of the tricuspid annulus and surrounding structures. RA: right atrium; RV: right ventricle; MV: mitral valve; AV: aortic valve.

The comprehensive assessment of the right heart and the adjacent anatomical structures, which the tricuspid defect could significantly remodel, provides an appropriate evaluation for TR severity, patients' clinical risk stratification, anatomical suitability for tricuspid interventions, and preprocedural planning in patients undergoing TV therapies [105]. Specifically, several fundamental parameters might be obtained by CT imaging in order to design the optimal procedure and achieve the highest success rate during transcatheter tricuspid valve interventions (TTVI), such as dimensions and morphology of the TV annulus, location of commissures, tethering parameters, anatomical regurgitant orifice area, right atrium (RA) and RV dimensions, surrounding structures, device landing zone, and vascular access routes [11]. Using multiplanar reconstruction, tricuspid cross-sectional area, perimeter, septolateral (SL), and anteroposterior (AP) diameters can be obtained by a short-axis view on the annular level. The SL diameter refers to the maximal distance in septal to the lateral direction (that corresponds to the anulus measurement in the four-chamber view at the transthoracic echocardiography), whereas the AP diameter is orthogonal to the previous one. Due to the complex saddle-shaped structure of the tricuspid annulus, a 2D approach does not precisely address the valvular anatomy. Therefore, 3D semiautomated software can help in this setting [108]. Moreover, dimensions are usually obtained both at end-systole and mid-diastole because of the dynamic variability in annular size. Interestingly, in a study by Praz et al., there was a good correspondence between TEE and CT for tricuspid annulus sizing and valve area in patients with severe TR [109]. Finally, distances between commissures (anteroseptal, posteroseptal, and anteroposterior) and distances between the centrum of the TV and commissures can also be measured [12].

The leaflet tethering is another important parameter to consider in TTVI planning. In a study by Van Rosendael et al. [110], in patients with TR $\geq$ 3+, CT exhibited greater tricuspid annulus and RV dimensions and marked tethering of the anterior and septal tricuspid leaflets compared to those with mild valvular defects. Of note, the grade of functional TR was independently correlated with the anteroposterior annulus diameter. The features of leaflet tethering, including tenting height, angle, and area, can be obtained with CT scan and compared to the ones visualized with echocardiography. The edge-to-edge repair using the Triclip (Abbott Vascular, Santa Clara, CA, USA) or PASCAL systems (Edwards Lifesciences, Irvine, CA, USA) allows bringing the TV leaflets closer, thus reducing the grade of regurgitation. The role of CT in the edge-to-edge repair is less important than the other techniques, even if viable information about the coaptation gap, annulus, and right chamber remodeling can be obtained [111].

Moreover, as described for the mitral valve, measuring the anatomical regurgitant orifice area (AROA) by CT is also feasible. It may be an additional grading tool for TR severity in patients with contradictory echocardiographic parameters [112]. Notably, this flow-independent parameter of TR severity provided by CT has been reported to strongly correlate with the 3D measurement of vena contracta (thus with three-dimensional assessment of the narrowest flow region of the tricuspid regurgitant volume), using trans-esophageal echocardiography [108]. The dimensions of the RV and RA are also crucial for evaluating the anatomic feasibility of transcatheter therapies. RA must allocate the delivery catheter and be large enough for various maneuvers during the procedure [11]. Furthermore, with the promising results of the trials regarding transcatheter TV replacement, assessing the right chambers is more important than ever. Some valves are used in high-risk patients, such as NaviGate bio prosthesis (NaviGate Cardiac Structures, Lake Forest) or EVOQUE valve (Edwards Lifesciences). In this setting, RV volume, the distance between the RV apex and the tricuspid annular plane, the location of the papillary muscles, the moderator band, and the presence of prominent trabeculae must be assessed with regard to the protrusion of the prosthesis into the RV, most notably to avoid RV outflow tract obstruction [111].

Tricuspid valve replacement is also challenging due to the lack of calcifications at the level of the tricuspid annulus [113]. The Melody prosthesis (Medtronic, Minneapolis) is usually used in transcatheter tricuspid valve-in-valve and valve-in-ring procedures. In this setting, 3D CT measurement of the effective inner diameters of the ring is fundamental to bypass the differences reported in the nominal size documented by surgical report [114]. Annuloplasty devices, such as Cardioband™ (Valtech Cardio, OrYehuda, Israel), use a transfemoral ring or suture-based approach to reduce the diameter in cases where annular dilation is the major pathophysiological mechanism. Therefore, in this type of transcatheter repair procedures, it is also essential to evaluate the structures surrounding the tricuspid annulus, particularly the course of the right coronary artery, that could be damaged. The vessel course in relation to the annulus is variable. An RCA course at the annular level was shown in 65% of patients, a superior (i.e., atrial) course in 10%, and a crossing course in 25% [115]. Finally, measurement of the inferior vena cava plays a role in some interventional procedures aiming to reduce TR. In the heterotopic implantation of valves in the caval veins, balloon-expandable transcatheter aortic valve prostheses such as Sapien XT (Edwards Lifesciences) are placed to reduce blood backflow and prevention of venous congestion. Other systems, such as the TricValve system (P&F, Vienna) or the Tricento (NVT AG, Muri), are deployed top-down from the superior to the inferior vena cava, improving pressure's profile in the right atrium. In these procedures, it is of crucial importance to calculate the distance between the junction plane of the inferior vena cava, the right atrium, and the first hepatic vein to avoid hepatic vein obstruction [12].

5. CT and Left Atrial Appendage

5.1. Anatomy of Left Atrial Appendage (LAA)

The left atrial appendage (LAA) is a finger-like projection from the body of the left atrium (LA). The junction is well defined by the presence of an orifice [116]. It is located on the anterior wall of the LA, and it extends to the lateral part of it, with the tip directed anterosuperiorly, with overlapping on the right ventricular outflow tract or the pulmonary trunk and the left main coronary vessel or the circumflex artery. The appendage overlies the atrioventricular groove and the left phrenic nerve courses over its covering fibrous pericardium [116]. Its orifice is usually elliptical, sometimes round, triangular, or water-drop shaped. The left ridge divides the orifice from the left pulmonary veins, whereas the muscular wall of the LA vestibule stands between the orifice and the mitral annulus [116]. LAA varies in size and shape; however, it is usually classified into four main types: "chicken wing" (the most common), "cactus" (30%), "windsock", and "cauliflower". The last one is the rarest but most associated with embolic events; it has a short overall length but a variable number of lobes without a dominant one [117]. Oppositely, the "chicken wing" shape is composed of a more prominent lobe that folds back on itself after it emerges from the orifice and could have secondary lobes [117]. The "cactus" shape has a dominant central lobe and secondary lobes emerging from it superiorly and inferiorly [118]. Finally, the "windsock" has a prominent lobe with multiple secondary and tertiary lobes with many variations in terms of localization [119].

5.2. Left Atrial Appendage Closure (LAAC)

In atrial fibrillation (AF), the LAA loses its contraction capability and undergoes a remodeling process that transforms it into a static pouch, with an increased risk of stagnation and thrombosis [120]. The risk of thrombosis is also higher in patients with left ventricular dysfunction and elevated left ventricular end-diastolic pressures, even without AF [121]. Traditionally, oral anticoagulation therapy has been the cornerstone of therapy for stroke prevention in patients with nonvalvular AF [122]. However, in some frailty patients, the increased bleeding risk associated with anticoagulation therapy might overcome the benefit of stroke prevention. Percutaneous left atrial appendage closure (LAAC) is a validated procedure that excludes the appendage with the use of dedicated devices. Two main devices are currently used in clinical practice: the Watchman (Boston Scientific), a parachute-shaped nitinol device with a permeable membrane over the atrial side and fixation barbs to secure it between the LAA walls, and the Amulet device, a self-expanding flexible nitinol mesh with a distal lobe, keeping hooks, and a proximal disk for sealing the LAA orifice. Both these devices have reported high post-procedural and long-term success rates of LAAC [123–125].

5.3. CT Assessment in LAA Transcatheter Closure

Multimodality imaging is essential for LAAC. MDCT allows a great resolution of LAA due to its minimal motion [126]. For patients in sinus rhythm, prospective electrocardiographic (ECG) gating is necessary by identifying either atrial systole/ventricular diastole or atrial diastole/ventricular systole. For patients in AF, retrospective ECG gating may be required, and the optimal reconstruction phase depends on the ventricular rate [127].

Computed tomography is particularly important in three phases regarding patients undergoing LAAC: the preprocedural exclusion of LA thrombosis, the preprocedural planning, taking into account LAA morphology and dimensions, and the surveillance after the procedure [126]. CT can easily exclude thrombi in the LAA, even if transesophageal echocardiography (TEE) remains the gold standard. A major strength of computed tomography is the high capability to exclude LAA thrombosis (96–100%) [128]. Delayed imaging allows the differentiation between the slow-flow sluggish and the thrombi; thus, the filling defect that persists after one minute of contrast injection is more suggestive of a real thrombus [129].

In the preprocedural planning of LAAC, the MDCT helps acquire information about LAA shape, size, and surrounding structures. Few studies compared computed tomography, transesophageal echocardiography, and angiography for LAA assessment. Most of them are retrospective, single-center studies, reporting larger dimensions with CT than 2D/3D-TEE and angiography. Rajwani et al. found that in 73 Watchman implantations, 2D-TEE and MDCT maximum diameter agreed on device size only in 25.4% of cases, mainly due to significative eccentricity of the orifice [130]. Notably, the LAAC device size choice depends on these measurements [126]. Computed tomography allows for determining LAA ostia and landing zones (the LAA zone where the LAAO device will ideally seat) and providing the minimum LAA diameter, maximum diameter, perimeter, and area. These measurements should be assessed at maximal LAA diastole or mid to late left ventricular systole, corresponding to maximum LAA end-diastolic filling. In this phase, the LAA is largest, thus reducing the risk of device undersizing and subsequent peri-device leaks. In a study by Wang et al., the CT-detected diameter of the LAA ostium calculated from the perimeter resulted in the best parameter for sizing the LAA occluder device [131]. It is essential to point out that different devices require different modalities of LAA ostium measurement [126]. For the Watchman, the landing zone is measured from the circumflex artery inferiorly to a superior point that is established at 1–2 cm within the left upper superior pulmonary vein ridge. For the Amplatzer Cardiac Plug (ACP) or the Amulet (second-generation ACP), the landing zone is usually placed 10 mm and 12–15 mm inward of the LAA orifice, respectively [126]. Once the LAA orifice diameters have been established, the LAA's depth must also be determined in the CT sagittal and coronal views. It is measured from the central point of the orifice to the apex of the main lobe, and the chosen device should have the same diameter as the LAA depth [126]. From a technical view, the assessment of the LAA shape is a valuable aid in predicting the level of difficulty of device implantation. The "chicken wing" shape is usually considered to be the most complicated, particularly in case of a proximal and sharp bend. "Cactus" and "cauliflower" shapes may be challenging compared with the "wind-sock" shape (Figure 12) [126].

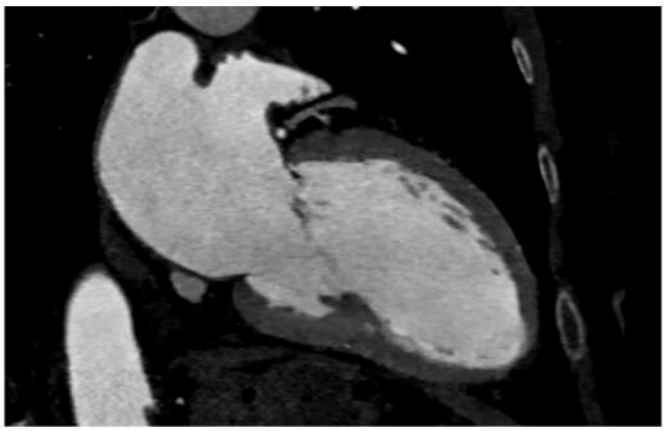

Figure 12. CT imaging for the assessment of left atrial appendage's conformation. Example of "chicken wing" shape.

Finally, MDCT has an important role in post-procedural follow-up, which can be performed 1–6 months after the device implantation. The primary role of computed tomography in this context is the exclusion of device-associated thrombus, post-implant device orientation, pericardial effusion, and peri-device leaks. Jaguszewski et al. found that CT detected leaks in 62% of cases in patients implanted with ACP, whereas TEE revealed only 36% [132]. A perpendicular position of the lobe in relation to the LAA neck has been reported to be a good predictor of the absence of residual leakage after the procedure; moreover, device compression of more than 10% is associated with complete sealing [133].

6. Conclusions

CT is a crucial imaging tool for structural cardiac disease interventions. Due to its high temporal and spatial resolution, cardiac CT has become fundamental for the preprocedural planning of THVI, allowing precise device sizing and vascular access assessment, helping with landing zone characterization, and reducing procedural complications. Ongoing indications for preprocedural computed tomography in cardiac interventional procedures include transcatheter aortic valve implantation, percutaneous interventions of the mitral, tricuspid, pulmonary valves, and left atrial appendage occlusion. The role of multimodality imaging will undoubtedly continue to grow because of the development of new software technologies that will allow integration of CT with other techniques [134–136], such as fluoroscopy in the catheterization laboratory. These advances will improve accuracy and safety in planning and guiding these interventions while reducing the dose of contrast volume, radiation exposure, and procedural duration.

Author Contributions: Conceptualization, A.N. and S.C.; validation, F.G., G.P.U.; writing—original draft preparation, A.N., S.C., E.N., A.D.F., L.V.; writing—review and editing, A.N., D.D.S.; visualization, F.P., V.C., F.M., E.R., R.M., R.R., C.C.Q.; supervision, G.P.U., F.G. All authors have read and agreed to the published version of the manuscript.

Funding: This research received no external funding.

Institutional Review Board Statement: Not applicable.

Informed Consent Statement: Not applicable.

Data Availability Statement: Not applicable.

Conflicts of Interest: The authors declare no conflict of interest.

References

1. Schoenhagen, P.; Numburi, U.; Halliburton, S.S.; Aulbach, P.; Von Roden, M.; Desai, M.Y.; Rodriguez, L.L.; Kapadia, S.R.; Tuzcu, E.M.; Lytle, B.W. Three-dimensional imaging in the context of minimally invasive and transcatheter cardiovascular interventions using multi-detector computed tomography: From pre-operative planning to intra-operative guidance. *Eur. Hear. J.* **2010**, *31*, 2727–2740. [CrossRef] [PubMed]
2. Boxt, L.M.; Lipton, M.J.; Kwong, R.Y.; Rybicki, F.; E Clouse, M. Computed tomography for assessment of cardiac chambers, valves, myocardium and pericardium. *Cardiol. Clin.* **2003**, *21*, 561–585. [CrossRef]
3. Ecabert, O.; Peters, J.; Schramm, H.; Lorenz, C.; von Berg, J.; Walker, M.J.; Vembar, M.; Olszewski, M.E.; Subramanyan, K.; Lavi, G.; et al. Automatic Model-Based Segmentation of the Heart in CT Images. *IEEE Trans. Med. Imaging* **2008**, *27*, 1189–1201. [CrossRef] [PubMed]
4. Hu, S.; Hoffman, E.; Reinhardt, J. Automatic lung segmentation for accurate quantitation of volumetric X-ray CT images. *IEEE Trans. Med. Imaging* **2001**, *20*, 490–498. [CrossRef] [PubMed]
5. Bae, K.T.; Giger, M.L.; Chen, C.; Kahn, C.E. Automatic segmentation of liver structure in CT images. *Med. Phys.* **1993**, *20*, 71–78. [CrossRef] [PubMed]
6. Mir, A.; Hanmandlu, M.; Tandon, S. Texture analysis of CT images. *IEEE Eng. Med. Biol. Mag.* **1995**, *14*, 781–786. [CrossRef]
7. Yang, X.; He, X.; Zhao, J.; Zhang, Y.; Zhang, S.; Xie, P. COVID-CT-Dataset: A CT Scan Dataset about COVID-19. *Mach. Learn.* **2020**. [CrossRef]
8. Sarma, A.; Heilbrun, M.E.; Conner, K.E.; Stevens, S.M.; Woller, S.C.; Elliott, C.G. Radiation and Chest CT Scan Examinations. *Chest* **2012**, *142*, 750–760. [CrossRef]
9. O'Connor, J.F.; Cohen, J.O. Computerized tomography (CAT scan, CT scan) in orthopaedic surgery. *JBJS* **1978**, *60*, 1096–1098. [CrossRef]
10. Patel, K.P.; Vandermolen, S.; Herrey, A.S.; Cheasty, E.; Menezes, L.; Moon, J.C.; Pugliese, F.; Treibel, T.A. Cardiac Computed Tomography: Application in Valvular Heart Disease. *Front. Cardiovasc. Med.* **2022**, *9*, 849540. [CrossRef]
11. Cammalleri, V.; Carpenito, M.; Bono, M.C.; Mega, S.; Ussia, G.P.; Grigioni, F. Transcatheter Tricuspid Valve Therapy: From Anatomy to Intervention. *Front. Cardiovasc. Med.* **2021**, *8*, 778445. [CrossRef] [PubMed]
12. Cammalleri, V.; Carpenito, M.; De Stefano, D.; Ussia, G.P.; Bono, M.C.; Mega, S.; Nusca, A.; Cocco, N.; Nobile, E.; De Filippis, A.; et al. Novel Computed Tomography Variables for Assessing Tricuspid Valve Morphology: Results from the TRIMA (Tricuspid Regurgitation IMAging) Study. *J. Clin. Med.* **2022**, *11*, 2825. [CrossRef] [PubMed]
13. Cammalleri, V.; Mega, S.; Ussia, G.P.; Grigioni, F. Mitral and Tricuspid Valves Percutaneous Repair in Patients with Advanced Heart Failure. *Hear. Fail. Clin.* **2021**, *17*, 607–618. [CrossRef] [PubMed]
14. Hell, M.M.; Achenbach, S. CT support of cardiac structural interventions. *Br. J. Radiol.* **2019**, *92*, 20180707. [CrossRef] [PubMed]

15. Piazza, N.; de Jaegere, P.; Schultz, C.; Becker, A.E.; Serruys, P.W.; Anderson, R.H. Anatomy of the Aortic Valvar Complex and Its Implications for Transcatheter Implantation of the Aortic Valve. *Circ. Cardiovasc. Interv.* **2008**, *1*, 74–81. [CrossRef] [PubMed]
16. Katsi, V.; Magkas, N.; Antonopoulos, A.; Trantalis, G.; Toutouzas, K.; Tousoulis, D. Aortic valve: Anatomy and structure and the role of vasculature in the degenerative process. *Acta Cardiol.* **2020**, *76*, 335–348. [CrossRef] [PubMed]
17. Kearney, L.; Ord, M.; Buxton, B.; Matalanis, G.; Patel, S.; Burrell, L.; Srivastava, P. Progression of aortic stenosis in elderly patients over long-term follow up. *Int. J. Cardiol.* **2012**, *167*, 1226–1231. [CrossRef]
18. Vahanian, A.; Beyersdorf, F.; Praz, F.; Milojevic, M.; Baldus, S.; Bauersachs, J.; Capodanno, D.; Conradi, L.; De Bonis, M.; De Paulis, R.; et al. *Multimodality Imaging for Transcatheter Aortic Valve Replacement*, 1st ed.; Springer: London, UK, 2014. [CrossRef]
19. Vahanian, A.; Beyersdorf, F.; Praz, F.; Milojevic, M.; Baldus, S.; Bauersachs, J.; Capodanno, D.; Conradi, L.; De Bonis, M.; De Paulis, R.; et al. 2021 ESC/EACTS Guidelines for the management of valvular heart disease. *Eur. Hear. J.* **2021**, *43*, 561–632. [CrossRef]
20. Tagliari, A.P.; Saadi, R.P.; Saadi, E.K. Transcatheter Aortic Valve Implantation for Pure Native Aortic Regurgitation: The Last Frontier. *J. Clin. Med.* **2022**, *11*, 5181. [CrossRef]
21. Nusca, A.; Bressi, E.; Colaiori, I.; Miglionico, M.; Di Sciascio, G. Antiplatelet therapy in valvular and structural heart disease interventions. *Cardiovasc. Diagn. Ther.* **2018**, *8*, 678–693. [CrossRef]
22. Ricottini, E.; Nusca, A.; Ussia, G.P.; Grigioni, F. Antithrombotic treatment for valve prostheses: Which drug, which dose, and when? *Prog. Cardiovasc. Dis.* **2022**, *72*, 4–14. [CrossRef]
23. Holmes, D.R.; Mack, M.J.; Kaul, S.; Agnihotri, A.; Alexander, K.P.; Bailey, S.R.; Calhoon, J.H.; Carabello, B.A.; Desai, M.Y.; Edwards, F.H.; et al. 2012 ACCF/AATS/SCAI/STS Expert Consensus Document on Transcatheter Aortic Valve Replacement. *J. Am. Coll. Cardiol.* **2012**, *59*, 1200–1254. [CrossRef]
24. Blanke, P.; Weir-McCall, J.R.; Achenbach, S.; Delgado, V.; Hausleiter, J.; Jilaihawi, H.; Marwan, M.; Norgaard, B.L.; Piazza, N.; Schoenhagen, P.; et al. Computed tomography imaging in the context of transcatheter aortic valve implantation (TAVI) / transcatheter aortic valve replacement (TAVR): An expert consensus document of the Society of Cardiovascular Computed Tomography. *J. Cardiovasc. Comput. Tomogr.* **2019**, *13*, 1–20. [CrossRef] [PubMed]
25. Chiocchi, M.; Ricci, F.; Pasqualetto, M.; D'errico, F.; Benelli, L.; Pugliese, L.; Cavallo, A.U.; Forcina, M.; Presicce, M.; De Stasio, V.; et al. Role of computed tomography in transcatheter aortic valve implantation and valve-in-valve implantation: Complete review of preprocedural and postprocedural imaging. *J. Cardiovasc. Med.* **2020**, *21*, 182–191. [CrossRef] [PubMed]
26. Binder, R.K.; Webb, J.G.; Willson, A.B.; Urena, M.; Hansson, N.C.; Norgaard, B.L.; Pibarot, P.; Barbanti, M.; Larose, E.; Freeman, M.; et al. The Impact of Integration of a Multidetector Computed Tomography Annulus Area Sizing Algorithm on Outcomes of Transcatheter Aortic Valve Replacement. *J. Am. Coll. Cardiol.* **2013**, *62*, 431–438. [CrossRef] [PubMed]
27. Corcione, N.; Morello, A.; Ferraro, P.; Cimmino, M.; Albanese, M.; Pepe, M.; Nestola, P.L.; Giordano, S.; Bardi, L.; Biondi-Zoccai, G.; et al. TAVI-CT score to evaluate the anatomic risk in patients undergoing transcatheter aortic valve implantation. *Sci. Rep.* **2022**, *12*, 1–9. [CrossRef]
28. Spaziano, M.; Chieffo, A.; Watanabe, Y.; Chandrasekhar, J.; Sartori, S.; Lefèvre, T.; Petronio, A.S.; Presbitero, P.; Tchetche, D.; Iadanza, A.; et al. Computed tomography predictors of mortality, stroke and conduction disturbances in women undergoing TAVR: A sub-analysis of the WIN-TAVI registry. *J. Cardiovasc. Comput. Tomogr.* **2018**, *12*, 338–343. [CrossRef]
29. Gama, F.; Teles, R.; Oliveira, A.; Brizido, C.; Goncalves, P.; Brito, J.; Ferreira, A.; Abecasis, J.; Almeida, M.; Mendes, M. Predicting pacemaker implantation after TAVR with procedural CT. *Eur. Hear. J.* **2020**, *41*, ehaa946.0192. [CrossRef]
30. Gegenava, T.; van der Bijl, P.; Hirasawa, K.; Vollema, E.M.; van Rosendael, A.; van der Kley, F.; de Weger, A.; Hautemann, D.J.; Reiber, J.H.; Marsan, N.A.; et al. Feature tracking computed tomography-derived left ventricular global longitudinal strain in patients with aortic stenosis: A comparative analysis with echocardiographic measurements. *J. Cardiovasc. Comput. Tomogr.* **2019**, *14*, 240–245. [CrossRef]
31. Masson, J.-B.; Kovac, J.; Schuler, G.; Ye, J.; Cheung, A.; Kapadia, S.; Tuzcu, M.E.; Kodali, S.; Leon, M.B.; Webb, J.G. Transcatheter Aortic Valve Implantation: Review of the Nature, Management, and Avoidance of Procedural Complications. *JACC: Cardiovasc. Interv.* **2009**, *2*, 811–820. [CrossRef]
32. Hayashida, K.; Lefèvre, T.; Chevalier, B.; Hovasse, T.; Romano, M.; Garot, P.; Mylotte, D.; Uribe, J.; Farge, A.; Donzeau-Gouge, P.; et al. Transfemoral Aortic Valve Implantation: New Criteria to Predict Vascular Complications. *JACC: Cardiovasc. Interv.* **2011**, *4*, 851–858. [CrossRef] [PubMed]
33. Okuyama, K.; Jilaihawi, H.; Kashif, M.; Takahashi, N.; Chakravarty, T.; Pokhrel, H.; Patel, J.; Forrester, J.S.; Nakamura, M.; Cheng, W.; et al. Transfemoral Access Assessment for Transcatheter Aortic Valve Replacement: Evidence-based application of computed tomography over invasive angiography. *Circ. Cardiovasc. Imaging* **2015**, *8*, e001995. [CrossRef] [PubMed]
34. Reardon, M.J.; Van Mieghem, N.M.; Popma, J.J.; Kleiman, N.S.; Søndergaard, L.; Mumtaz, M.; Adams, D.H.; Deeb, G.M.; Maini, B.; Gada, H.; et al. Surgical or Transcatheter Aortic-Valve Replacement in Intermediate-Risk Patients. *N. Engl. J. Med.* **2017**, *376*, 1321–1331. [CrossRef] [PubMed]
35. Lehmkuhl, L.; Foldyna, B.; Haensig, M.; Von Aspern, K.; Lücke, C.; Andres, C.; Grothoff, M.; Riese, F.; Nitzsche, S.; Holzhey, D.; et al. Role of preprocedural computed tomography in transcatheter aortic valve implantation. *Fortschr. Geb. Rontgenstr. Nuklearmed.* **2013**, *185*, 941–949. [CrossRef]
36. Jurencak, T.; Turek, J.; Kietselaer, B.L.J.H.; Mihl, C.; Kok, M.; Van Ommen, V.G.V.A.; Van Garsse, L.A.F.M.; Nijssen, E.C.; Wildberger, J.E.; Das, M. MDCT evaluation of aortic root and aortic valve prior to TAVI. What is the optimal imaging time point in the cardiac cycle? *Eur. Radiol.* **2015**, *25*, 1975–1983. [CrossRef]

37. Adams, D.H.; Popma, J.J.; Reardon, M.J.; Yakubov, S.J.; Coselli, J.S.; Deeb, G.M.; Gleason, T.G.; Buchbinder, M.; Hermiller, J., Jr.; Kleiman, N.S.; et al. Transcatheter Aortic-Valve Replacement with a Self-Expanding Prosthesis. *N. Engl. J. Med.* **2014**, *370*, 1790–1798. [CrossRef]
38. Mack, M.J.; Leon, M.B.; Thourani, V.H.; Makkar, R.; Kodali, S.K.; Russo, M.; Kapadia, S.R.; Malaisrie, S.C.; Cohen, D.J.; Pibarot, P.; et al. Transcatheter Aortic-Valve Replacement with a Balloon-Expandable Valve in Low-Risk Patients. *N. Engl. J. Med.* **2019**, *380*, 1695–1705. [CrossRef]
39. Mylotte, D.; Dorfmeister, M.; Elhmidi, Y.; Mazzitelli, D.; Bleiziffer, S.; Wagner, A.; Noterdaeme, T.; Lange, R.; Piazza, N. Erroneous Measurement of the Aortic Annular Diameter Using 2-Dimensional Echocardiography Resulting in Inappropriate CoreValve Size Selection: A retrospective comparison with multislice computed tomography. *JACC: Cardiovasc. Interv.* **2014**, *7*, 652–661. [CrossRef]
40. Helmy, S.M.; Karim, S.A. Multimodality imaging in aortic stenosis. *Hear. Views* **2022**, *23*, 22. [CrossRef]
41. Vincent, F.; Ternacle, J.; Denimal, T.; Shen, M.; Redfors, B.; Delhaye, C.; Simonato, M.; Debry, N.; Verdier, B.; Shahim, B.; et al. Transcatheter Aortic Valve Replacement in Bicuspid Aortic Valve Stenosis. *Circulation* **2021**, *143*, 1043–1061. [CrossRef]
42. Tanaka, R.; Yoshioka, K.; Niinuma, H.; Ohsawa, S.; Okabayashi, H.; Ehara, S. Diagnostic Value of Cardiac CT in the Evaluation of Bicuspid Aortic Stenosis: Comparison With Echocardiography and Operative Findings. *Am. J. Roentgenol.* **2010**, *195*, 895–899. [CrossRef] [PubMed]
43. Popma, J.J.; Ramadan, R. CT Imaging of Bicuspid Aortic Valve Disease for TAVR ∗. *JACC: Cardiovasc. Imaging* **2016**, *9*, 1159–1163. [CrossRef] [PubMed]
44. Doris, M.K.; Jenkins, W.; Robson, P.; Pawade, T.; Andrews, J.P.; Bing, R.; Cartlidge, T.; Shah, A.; Pickering, A.; Williams, M.C.; et al. Computed tomography aortic valve calcium scoring for the assessment of aortic stenosis progression. *Heart* **2020**, *106*, 1906–1913. [CrossRef]
45. Feuchtner, G.M.; Müller, S.; Grander, W.; Alber, H.F.; Bartel, T.; Friedrich, G.J.; Reinthaler, M.; Pachinger, O.; Nedden, D.Z.; Dichtl, W. Aortic valve calcification as quantified with multislice computed tomography predicts short-term clinical outcome in patients with asymptomatic aortic stenosis. *J. Hear. Valve Dis.* **2006**, *15*, 494–498.
46. Rosenhek, R.; Binder, T.; Porenta, G.; Lang, I.; Christ, G.; Schemper, M.; Maurer, G.; Baumgartner, H. Predictors of Outcome in Severe, Asymptomatic Aortic Stenosis. *New Engl. J. Med.* **2000**, *343*, 611–617. [CrossRef] [PubMed]
47. Leber, A.W.; Kasel, M.; Ischinger, T.; Ebersberger, U.H.; Antoni, D.; Schmidt, M.; Riess, G.; Renz, V.; Huber, A.; Helmberger, T.; et al. Aortic valve calcium score as a predictor for outcome after TAVI using the CoreValve revalving system. *Int. J. Cardiol.* **2011**, *166*, 652–657. [CrossRef]
48. Haensig, M.; Lehmkuhl, L.; Rastan, A.J.; Kempfert, J.; Mukherjee, C.; Gutberlet, M.; Holzhey, D.; Mohr, F.W. Aortic valve calcium scoring is a predictor of significant paravalvular aortic insufficiency in transapical-aortic valve implantation. *Eur. J. Cardio-Thoracic Surg.* **2012**, *41*, 1234–1241. [CrossRef]
49. Lee, J.A.; Singh, T.; Ben Dor, I.; Torguson, R.; Okubagzi, P.; Satler, L.; Goldstein, S.; Taylor, A.; Weigold, W.G.; Pichard, A.; et al. AAortic valve calcium score by computed tomography in predicting perivalvular aortic insufficiency post transcatheter aortic valve implantation (TAVI). *J. Am. Coll. Cardiol.* **2012**, *59*, E1962. [CrossRef]
50. Unbehaun, A.; Pasic, M.; Dreysse, S.; Drews, T.; Kukucka, M.; Mladenow, A.; Ivanitskaja-Kühn, E.; Hetzer, R.; Buz, S. Transapical Aortic Valve Implantation: Incidence and predictors of paravalvular leakage and transvalvular regurgitation in a series of 358 patients. *J. Am. Coll. Cardiol.* **2012**, *59*, 211–221. [CrossRef]
51. Feuchtner, G.; Plank, F.; Bartel, T.; Mueller, S.; Leipsic, J.; Schachner, T.; Müller, L.; Friedrich, G.; Klauser, A.; Grimm, M.; et al. Prediction of Paravalvular Regurgitation After Transcatheter Aortic Valve Implantation by Computed Tomography: Value of Aortic Valve and Annular Calcification. *Ann. Thorac. Surg.* **2013**, *96*, 1574–1580. [CrossRef]
52. Ribeiro, H.B.; Nombela-Franco, L.; Urena, M.; Mok, M.; Pasian, S.; Doyle, D.; DeLarochellière, R.; Côté, M.; Laflamme, L.; DeLarochellière, H.; et al. Coronary Obstruction Following Transcatheter Aortic Valve Implantation: A systematic review. *JACC: Cardiovasc. Interv.* **2013**, *6*, 452–461. [CrossRef] [PubMed]
53. Jilaihawi, H.; Chin, D.; Spyt, T.; Jeilan, M.; Vasa-Nicotera, M.; Bence, J.; Logtens, E.; Kovac, J. Prosthesis-patient mismatch after transcatheter aortic valve implantation with the Medtronic-Corevalve bioprosthesis. *Eur. Heart J.* **2009**, *31*, 857–864. [CrossRef] [PubMed]
54. Delgado, V.; Ng, A.C.T.; Shanks, M.; Van Der Kley, F.; Schuijf, J.D.; Van De Veire, N.R.L.; Kroft, L.; De Roos, A.; Schalij, M.J.; Bax, J.J. Transcatheter aortic valve implantation: Role of multimodality cardiac imaging. *Expert Rev. Cardiovasc. Ther.* **2010**, *8*, 113–123. [CrossRef]
55. Piazza, N.; Nuis, R.-J.; Tzikas, A.; Otten, A.; Onuma, Y.; García-García, H.; Schultz, C.; van Domburg, R.; van Es, G.-A.; van Geuns, R.; et al. Persistent conduction abnormalities and requirements for pacemaking six months after transcatheter aortic valve implantation. *Eurointervention* **2010**, *6*, 475–484. [CrossRef] [PubMed]
56. Jilaihawi, H.; Chin, D.; Vasa-Nicotera, M.; Jeilan, M.; Spyt, T.; Ng, G.A.; Bence, J.; Logtens, E.; Kovac, J. Predictors for permanent pacemaker requirement after transcatheter aortic valve implantation with the CoreValve bioprosthesis. *Am. Hear. J.* **2009**, *157*, 860–866. [CrossRef] [PubMed]
57. Moreno, R.; Calvo, L.; García, E.; Dobarro, D. Severe septal hypertrophy: Is it necessarily a contraindication for the transcatheter implantation of an Edwards-Sapien prosthesis? *Rev. Esp. Cardiol.* **2010**, *63*, 241–242. [CrossRef] [PubMed]

58. Stolzmann, P.; Scheffel, H.; Trindade, P.T.; Plass, A.R.; Husmann, L.; Leschka, S.; Genoni, M.; Marincek, B.; Kaufmann, P.A.; Alkadhi, H. Left Ventricular and Left Atrial Dimensions and Volumes: Comparison between dual-source CT and echo-cardiography. *Investig. Radiol.* **2008**, *43*, 284–289. [CrossRef] [PubMed]
59. Okuno, T.; Asami, M.; Heg, D.; Lanz, J.; Praz, F.; Hagemeyer, D.; Brugger, N.; Gräni, C.; Huber, A.; Spirito, A.; et al. Impact of Left Ventricular Outflow Tract Calcification on Procedural Outcomes After Transcatheter Aortic Valve Replacement. *JACC: Cardiovasc. Interv.* **2020**, *13*, 1789–1799. [CrossRef]
60. Maréchaux, S.; Illman, J.E.; Huynh, J.; Michelena, H.I.; Nkomo, V.T.; Tribouilloy, C. Functional anatomy and pathophysiologic principles in mitral regurgitation: Non-invasive assessment. *Prog. Cardiovasc. Dis.* **2017**, *60*, 289–304. [CrossRef]
61. Komoda, T.; Hetzer, R.; Oellinger, J.; Siniawski, H.; Hofmeister, J.; Hübler, M.; Felix, R.; Uyama, C.; Maeta, H. Mitral Annular Flexibility. *J. Card. Surg.* **1997**, *12*, 102–109. [CrossRef]
62. Millington-Sanders, C.; Meir, A.; Lawrence, L.; Stolinski, C. Structure of chordae tendineae in the left ventricle of the human heart. *J. Anat.* **1998**, *192*, 573–581. [CrossRef] [PubMed]
63. Ranganathan, N.; Lam, J.H.C.; Wigle, E.D.; Silver, M.D. Morphology of the Human Mitral Valve. *Circulation* **1970**, *41*, 459–467. [CrossRef] [PubMed]
64. Lam, J.H.C.; Ranganathan, N.; Wigle, E.D.; Silver, M.D. Morphology of the Human Mitral Valve. *Circulation* **1970**, *41*, 449–458. [CrossRef] [PubMed]
65. Nkomo, V.T.; Gardin, J.M.; Skelton, T.N.; Gottdiener, J.S.; Scott, C.G.; Enriquez-Sarano, M. Burden of valvular heart diseases: A population-based study. *Lancet* **2006**, *368*, 1005–1011. [CrossRef] [PubMed]
66. Delgado, V.; Tops, L.F.; Schuijf, J.D.; de Roos, A.; Brugada, J.; Schalij, M.J.; Thomas, J.D.; Bax, J.J. Assessment of Mitral Valve Anatomy and Geometry With Multislice Computed Tomography. *JACC: Cardiovasc. Imaging* **2009**, *2*, 556–565. [CrossRef]
67. Regueiro, A.; Granada, J.F.; Dagenais, F.; Rodés-Cabau, J. Transcatheter Mitral Valve Replacement. *J. Am. Coll. Cardiol.* **2017**, *69*, 2175–2192. [CrossRef]
68. Maisano, F.; Torracca, L.; Oppizzi, M.; Stefano, P.; D'Addario, G.; La Canna, G.; Zogno, M.; Alfieri, O. The edge-to-edge technique: A simplified method to correct mitral insufficiency1. *Eur. J. Cardio-Thoracic Surg.* **1998**, *13*, 240–246. [CrossRef] [PubMed]
69. Feldman, T.; Foster, E.; Glower, D.D.; Kar, S.; Rinaldi, M.J.; Fail, P.S.; Smalling, R.W.; Siegel, R.; Rose, G.A.; Engeron, E.; et al. Percutaneous Repair or Surgery for Mitral Regurgitation. *New Engl. J. Med.* **2011**, *364*, 1395–1406. [CrossRef]
70. Feldman, T.; Lim, S.; Fail, P.; Whisenant, B.; Rinaldi, M.; Grayburn, P.; Smalling, R.; Foster, E.; Weissman, N.; Kar, S. Everest ii realism—a continued access study to evaluate the safety and effectiveness of the mitraclip device: Analysis of results through 1 year. *J. Am. Coll. Cardiol.* **2015**, *65*, A1983. [CrossRef]
71. Stone, G.W.; Lindenfeld, J.; Abraham, W.T.; Kar, S.; Lim, D.S.; Mishell, J.M.; Whisenant, B.; Grayburn, P.A.; Rinaldi, M.; Kapadia, S.R.; et al. Transcatheter Mitral-Valve Repair in Patients with Heart Failure. *N. Engl. J. Med.* **2018**, *379*, 2307–2318. [CrossRef]
72. Faggioni, L.; Gabelloni, M.; Accogli, S.; Angelillis, M.; Costa, G.; Spontoni, P.; Petronio, A.S.; Caramella, D. Preprocedural planning of transcatheter mitral valve interventions by multidetector CT: What the radiologist needs to know. *Eur. J. Radiol. Open* **2018**, *5*, 131–140. [CrossRef] [PubMed]
73. Feuchtner, G.M.; Alkadhi, H.; Karlo, C.; Sarwar, A.; Meier, A.; Dichtl, W.; Leschka, S.; Blankstein, R.; Gruenenfelder, J.; Stolzmann, P.; et al. Cardiac CT Angiography for the Diagnosis of Mitral Valve Prolapse: Comparison with Echocardiography. *Radiology* **2010**, *254*, 374–383. [CrossRef] [PubMed]
74. Lee, A.P.-W.; Jin, C.-N.; Fan, Y.; Wong, R.H.; Underwood, M.J.; Wan, S. Functional Implication of Mitral Annular Disjunction in Mitral Valve Prolapse. *JACC: Cardiovasc. Imaging* **2017**, *10*, 1424–1433. [CrossRef] [PubMed]
75. Ewe, S.H.; Klautz, R.J.; Schalij, M.J.; Delgado, V. Role of computed tomography imaging for transcatheter valvular repair/insertion. *Int. J. Cardiovasc. Imaging* **2011**, *27*, 1179–1193. [CrossRef]
76. Naoum, C.; Leipsic, J.; Cheung, A.; Ye, J.; Bilbey, N.; Mak, G.; Berger, A.; Dvir, D.; Arepalli, C.; Grewal, J.; et al. Mitral Annular Dimensions and Geometry in Patients With Functional Mitral Regurgitation and Mitral Valve Prolapse. *JACC: Cardiovasc. Imaging* **2016**, *9*, 269–280. [CrossRef]
77. Nishimura, R.A.; Bonow, R.O. Percutaneous Repair of Secondary Mitral Regurgitation—A Tale of Two Trials. *New Engl. J. Med.* **2018**, *379*, 2374–2376. [CrossRef]
78. E van Wijngaarden, S.; Kamperidis, V.; Regeer, M.V.; Palmen, M.; Schalij, M.J.; Klautz, R.J.; Bax, J.J.; Marsan, N.A.; Delgado, V. Three-dimensional assessment of mitral valve annulus dynamics and impact on quantification of mitral regurgitation. *Eur. Hear. J. Cardiovasc. Imaging* **2017**, *19*, 176–184. [CrossRef]
79. Palmisano, A.; Nicoletti, V.; Colantoni, C.; Monti, C.B.; Pannone, L.; Vignale, D.; Darvizeh, F.; Agricola, E.; Schaffino, S.; De Cobelli, F.; et al. Dynamic changes of mitral valve annulus geometry at preprocedural CT: Relationship with functional classes of regurgitation. *Eur. Radiol. Exp.* **2021**, *5*, 1–12. [CrossRef]
80. Ranganath, P.; Moore, A.; Guerrero, M.; Collins, J.; Foley, T.; Williamson, E.; Rajiah, P. CT for Pre- and Postprocedural Evaluation of Transcatheter Mitral Valve Replacement. *Radiographics* **2020**, *40*, 1528–1553. [CrossRef]
81. Blanke, P.; Dvir, D.; Cheung, A.; Ye, J.; Levine, R.A.; Precious, B.; Berger, A.; Stub, D.; Hague, C.; Murphy, D.; et al. A simplified D-shaped model of the mitral annulus to facilitate CT-based sizing before transcatheter mitral valve implantation. *J. Cardiovasc. Comput. Tomogr.* **2014**, *8*, 459–467. [CrossRef]

82. Blanke, P.; Naoum, C.; Webb, J.; Dvir, D.; Hahn, R.T.; Grayburn, P.; Moss, R.R.; Reisman, M.; Piazza, N.; Leipsic, J. Multimodality Imaging in the Context of Transcatheter Mitral Valve Replacement. *JACC: Cardiovasc. Imaging* **2015**, *8*, 1191–1208. [CrossRef] [PubMed]
83. Wang, D.D.; Eng, M.H.; Greenbaum, A.; Myers, E.; Forbes, M.; Karabon, P.; Pantelic, M.; Song, T.; Nadig, J.; Guerrero, M.; et al. Validating a prediction modeling tool for left ventricular outflow tract (LVOT) obstruction after transcatheter mitral valve replacement (TMVR). *Catheter. Cardiovasc. Interv.* **2017**, *92*, 379–387. [CrossRef]
84. Yoon, S.-H.; Bleiziffer, S.; Latib, A.; Eschenbach, L.; Ancona, M.; Vincent, F.; Kim, W.-K.; Unbehaum, A.; Asami, M.; Dhoble, A.; et al. Predictors of Left Ventricular Outflow Tract Obstruction After Transcatheter Mitral Valve Replacement. *JACC: Cardiovasc. Interv.* **2019**, *12*, 182–193. [CrossRef] [PubMed]
85. Guerrero, M.; Salinger, M.; Pursnani, A.; Pearson, P.; Lampert, M.; Levisay, J.; Russell, H.; Feldman, T. Transseptal transcatheter mitral valve-in-valve: A step by step guide from preprocedural planning to postprocedural care. *Catheter. Cardiovasc. Interv.* **2017**, *92*, E185–E196. [CrossRef]
86. Gersh, B.J.; Maron, B.J.; Bonow, R.O.; Dearani, J.A.; Fifer, M.A.; Link, M.S.; Naidu, S.S.; Nishimura, R.A.; Ommen, S.R.; Rakowski, H.; et al. 2011 ACCF/AHA Guideline for the Diagnosis and Treatment of Hypertrophic Cardiomyopathy. *Circulation* **2011**, *124*, e783–e831. [CrossRef]
87. Babaliaros, V.C.; Greenbaum, A.B.; Khan, J.M.; Rogers, T.; Wang, D.D.; Eng, M.H.; O'Neill, W.W.; Paone, G.; Thourani, V.H.; Lerakis, S.; et al. Intentional Percutaneous Laceration of the Anterior Mitral Leaflet to Prevent Outflow Obstruction During Transcatheter Mitral Valve Replacement. *JACC: Cardiovasc. Interv.* **2017**, *10*, 798–809. [CrossRef]
88. Faletra, F.F.; Leo, L.A.; Paiocchi, V.L.; Caretta, A.; Viani, G.M.; Schlossbauer, S.A.; Demertzis, S.; Ho, S.Y. Anatomy of mitral annulus insights from non-invasive imaging techniques. *Eur. Hear. J. Cardiovasc. Imaging* **2019**, *20*, 843–857. [CrossRef]
89. Thaden, J.J.; Malouf, J.F.; Nkomo, V.T.; Pislaru, S.V.; Holmes, D.R.; Reeder, G.S.; Rihal, C.S.; Eleid, M.F. Mitral Valve Anatomic Predictors of Hemodynamic Success With Transcatheter Mitral Valve Repair. *J. Am. Hear. Assoc.* **2018**, *7*, e007315. [CrossRef] [PubMed]
90. Grover, R.; Ohana, M.; Arepalli, C.D.; Sellers, S.L.; Mooney, J.; Kueh, S.-H.; Kim, U.; Blanke, P.; Leipsic, J.A. Role of MDCT Imaging in Planning Mitral Valve Intervention. *Curr. Cardiol. Rep.* **2018**, *20*, 16. [CrossRef] [PubMed]
91. Natarajan, N.; Patel, P.; Bartel, T.; Kapadia, S.; Navia, J.; Stewart, W.; Tuzcu, E.M.; Schoenhagen, P. Peri-procedural imaging for transcatheter mitral valve replacement. *Cardiovasc. Diagn. Ther.* **2016**, *6*, 144–159. [CrossRef]
92. Storz, C.; Mangold, S.; Mueller, K.A.; Lausberg, H.; Gatidis, S.; Heber, S.D.; Schlett, C.L.; Nikolaou, K.; Bamberg, F. Cardiac CT for Guiding Mitral Valve Interventions. *Curr. Cardiovasc. Imaging Rep.* **2017**, *10*, 1–10. [CrossRef]
93. Rottländer, D.; Ballof, J.; Gödde, M.; Degen, H.; Ögütcü, A.; Alektorov, K.; Chatrou, M.; Heintzen, M.P.; Haude, M. CT-Angiography to predict outcome after indirect mitral annuloplasty in patients with functional mitral regurgitation. *Catheter. Cardiovasc. Interv.* **2020**, *97*, 495–502. [CrossRef]
94. Rottländer, D.; Gödde, M.; Degen, H.; Ögütcü, A.; Saal, M.; Haude, M. Procedural planning of CS -based indirect mitral annuloplasty using CT-angiography. *Catheter. Cardiovasc. Interv.* **2021**, *98*, 1393–1401. [CrossRef] [PubMed]
95. Urena, M.; Himbert, D.; Brochet, E.; Carrasco, J.L.; Iung, B.; Nataf, P.; Vahanian, A. Transseptal Transcatheter Mitral Valve Replacement Using Balloon-Expandable Transcatheter Heart Valves. *JACC: Cardiovasc. Interv.* **2017**, *10*, 1905–1919. [CrossRef] [PubMed]
96. Hosoba, S.; Mori, M.; Goto, Y.; Fukumoto, Y.; Shimura, T.; Yamamoto, M. Hypo-attenuated leaflet thickening in surgically-implanted mitral bioprosthesis. *J. Cardiothorac. Surg.* **2020**, *15*, 74–77. [CrossRef] [PubMed]
97. Kaewkes, D.; Patel, V.; Ochiai, T.; Flint, N.; Ahmad, Y.; Kim, I.; Koseki, K.; Sharma, R.; Joseph, J.; Yoon, S.-H.; et al. Usefulness of Computed Tomography to Predict Mitral Stenosis After Transcatheter Mitral Valve Edge-to-Edge Repair. *Am. J. Cardiol.* **2021**, *153*, 109–118. [CrossRef] [PubMed]
98. Dahou, A.; Levin, D.; Reisman, M.; Hahn, R.T. Anatomy and Physiology of the Tricuspid Valve. *JACC: Cardiovasc. Imaging* **2019**, *12*, 458–468. [CrossRef] [PubMed]
99. Taramasso, M.; Pozzoli, A.; Basso, C.; Thiene, G.; Denti, P.; Kuwata, S.; Nietlispach, F.; Alfieri, O.; Hahn, R.T.; Nickenig, G.; et al. Compare and contrast tricuspid and mitral valve anatomy: Interventional perspectives for transcatheter tricuspid valve therapies. *Eurointervention* **2018**, *13*, 1889–1898. [CrossRef]
100. Mangieri, A.; Sticchi, A.; Gohar, A.; Regazzoli, D.; Fazzari, F.; Pini, D.; Pellegrino, M.; Pagliaro, B.; Loiacono, F.; Chiarito, M.; et al. Percutaneous Tricuspid Valve Repair. *Rev. Cardiovasc. Med.* **2022**, *23*, 220. [CrossRef]
101. Oliveira, D.C.; Oliveira, C.G. The Forgotten, Not Studied or Not Valorized Tricuspid Valve: The Transcatheter Revolution Is Coming. *Cardiol. Res.* **2019**, *10*, 199–206. [CrossRef]
102. Topilsky, Y.; Maltais, S.; Medina-Inojosa, J.; Oguz, D.; Michelena, H.; Maalouf, J.; Mahoney, D.W.; Enriquez-Sarano, M. Burden of Tricuspid Regurgitation in Patients Diagnosed in the Community Setting. *JACC Cardiovasc. Imaging* **2019**, *12*, 433–442. [CrossRef]
103. Benfari, G.; Antoine, C.; Miller, W.L.; Thapa, P.; Topilsky, Y.; Rossi, A.; Michelena, H.I.; Pislaru, S.; Enriquez-Sarano, M. Excess Mortality Associated With Functional Tricuspid Regurgitation Complicating Heart Failure With Reduced Ejection Fraction. *Circulation* **2019**, *140*, 196–206. [CrossRef] [PubMed]
104. Praz, F.; Muraru, D.; Kreidel, F.; Lurz, P.; Hahn, R.T.; Delgado, V.; Senni, M.; von Bardeleben, R.S.; Nickenig, G.; Hausleiter, J.; et al. Transcatheter treatment for tricuspid valve disease. *Eurointervention* **2021**, *17*, 791–808. [CrossRef] [PubMed]

105. Hashimoto, G.; Fukui, M.; Sorajja, P.; Cavalcante, J.L. Essential roles for CT and MRI in timing of therapy in tricuspid regurgitation. *Prog. Cardiovasc. Dis.* **2019**, *62*, 459–462. [CrossRef] [PubMed]
106. Lewis, M.A.; Pascoal, A.; Keevil, S.F.; Lewis, C.A. Selecting a CT scanner for cardiac imaging: The heart of the matter. *Br. J. Radiol.* **2016**, *89*, 20160376. [CrossRef] [PubMed]
107. Pulerwitz, T.C.; Khalique, O.K.; Leb, J.; Hahn, R.T.; Nazif, T.; Leon, M.B.; George, I.; Vahl, T.P.; D'Souza, B.; Bapat, V.N.; et al. Optimizing Cardiac CT Protocols for Comprehensive Acquisition Prior to Percutaneous MV and TV Repair/Replacement. *JACC: Cardiovasc. Imaging* **2020**, *13*, 836–850. [CrossRef]
108. Lopes, B.B.; Sorajja, P.; Hashimoto, G.; Fukui, M.; Bapat, V.N.; Du, Y.; Bae, R.; Schwartz, R.S.; Stanberry, L.I.; Enriquez-Sarano, M.; et al. Tricuspid Anatomic Regurgitant Orifice Area by Functional DSCT. *JACC: Cardiovasc. Imaging* **2021**, *14*, 1669–1672. [CrossRef]
109. Praz, F.; Khalique, O.K.; Macedo, L.G.D.R.; Pulerwitz, T.C.; Jantz, J.; Wu, I.Y.; Kantor, A.; Patel, A.; Vahl, T.; Bapat, V.; et al. Comparison between Three-Dimensional Echocardiography and Computed Tomography for Comprehensive Tricuspid Annulus and Valve Assessment in Severe Tricuspid Regurgitation: Implications for Tricuspid Regurgitation Grading and Transcatheter Therapies. *J. Am. Soc. Echocardiogr.* **2018**, *31*, 1190–1202.e3. [CrossRef]
110. van Rosendael, P.J.; Joyce, E.; Katsanos, S.; Debonnaire, P.; Kamperidis, V.; van der Kley, F.; Schalij, M.J.; Bax, J.J.; Marsan, N.A.; Delgado, V. Tricuspid valve remodelling in functional tricuspid regurgitation: Multidetector row computed tomography insights. *Eur. Hear. J. Cardiovasc. Imaging* **2015**, *17*, 96–105. [CrossRef]
111. Hell, M.M.; Emrich, T.; Kreidel, F.; Kreitner, K.-F.; Schoepf, U.J.; Münzel, T.; von Bardeleben, R.S. Computed tomography imaging needs for novel transcatheter tricuspid valve repair and replacement therapies. *Eur. Hear. J. Cardiovasc. Imaging* **2020**, *22*, 601–610. [CrossRef]
112. Hahn, R.T.; Thomas, J.D.; Khalique, O.K.; Cavalcante, J.L.; Praz, F.; Zoghbi, W.A. Imaging Assessment of Tricuspid Regurgitation Severity. *JACC: Cardiovasc. Imaging* **2019**, *12*, 469–490. [CrossRef] [PubMed]
113. Fukuda, S.; Saracino, G.; Matsumura, Y.; Daimon, M.; Tran, H.; Greenberg, N.L.; Hozumi, T.; Yoshikawa, J.; Thomas, J.D.; Shiota, T. Three-Dimensional Geometry of the Tricuspid Annulus in Healthy Subjects and in Patients With Functional Tricuspid Regurgitation. *Circulation* **2006**, *114*, I492–I498. [CrossRef] [PubMed]
114. McElhinney, D.B.; Cabalka, A.K.; Aboulhosn, J.A.; Eicken, A.; Boudjemline, Y.; Schubert, S.; Himbert, D.; Asnes, J.D.; Salizzoni, S.; Bocks, M.L.; et al. Transcatheter Tricuspid Valve-in-Valve Implantation for the Treatment of Dysfunctional Surgical Bioprosthetic Valves: An International, Multicenter Registry Study. *Circulation* **2016**, *133*, 1582–1593. [CrossRef] [PubMed]
115. van Rosendael, P.J.; Kamperidis, V.; Kong, W.K.; van Rosendael, A.R.; van der Kley, F.; Marsan, N.A.; Delgado, V.; Bax, J.J. Computed tomography for planning transcatheter tricuspid valve therapy. *Eur. Hear. J.* **2016**, *38*, 665–674. [CrossRef] [PubMed]
116. Delgado, V.; Di Biase, L.; Leung, M.; Romero, J.; Tops, L.F.; Casadei, B.; Marrouche, N.; Bax, J.J. Structure and Function of the Left Atrium and Left Atrial Appendage. *J. Am. Coll. Cardiol.* **2017**, *70*, 3157–3172. [CrossRef] [PubMed]
117. Di Biase, L.; Santangeli, P.; Anselmino, M.; Mohanty, P.; Salvetti, I.; Gili, S.; Horton, R.; Sanchez, J.E.; Bai, R.; Mohanty, S.; et al. Does the Left Atrial Appendage Morphology Correlate With the Risk of Stroke in Patients With Atrial Fibrillation? *J. Am. Coll. Cardiol.* **2012**, *60*, 531–538. [CrossRef] [PubMed]
118. Karim, N.; Ho, S.Y.; Nicol, E.; Li, W.; Zemrak, F.; Markides, V.; Reddy, V.; Wong, T. The left atrial appendage in humans: Structure, physiology, and pathogenesis. *Eur.* **2019**, *22*, 5–18. [CrossRef]
119. Romero, J.; Natale, A.; Di Biase, L. Left Atrial Appendage Morphology and Physiology: "The Missing Piece in the Puzzle". *J. Cardiovasc. Electrophysiol.* **2015**, *26*, 928–933. [CrossRef]
120. Shirani, J.; Alaeddini, J. Structural Remodeling of the Left Atrial Appendage in Patients with Chronic Non-Valvular Atrial Fibrillation. *Cardiovasc. Pathol.* **2000**, *9*, 95–101. [CrossRef]
121. Vigna, C.; Russo, A.; De Rito, V.; Perna, G.; Villella, A.; Testa, M.; Sollazzo, V.; Fanelli, R.; Loperfido, F. Frequency of left atrial thrombi by transesophageal echocardiography in idiopathic and in ischemic dilated cardiomyopathy. *Am. J. Cardiol.* **1992**, *70*, 1500–1501. [CrossRef]
122. Crandall, M.A.; Bradley, D.J.; Packer, D.L.; Asirvatham, S.J. Contemporary Management of Atrial Fibrillation: Update on Anticoagulation and Invasive Management Strategies. *Mayo Clin. Proc.* **2009**, *84*, 643–662. [CrossRef] [PubMed]
123. Fountain, R.B.; Holmes, D.R.; Chandrasekaran, K.; Packer, D.; Asirvatham, S.; Van Tassel, R.; Turi, Z. The PROTECT AF (WATCHMAN Left Atrial Appendage System for Embolic PROTECTion in Patients with Atrial Fibrillation) Trial. *Am. Hear. J.* **2006**, *151*, 956–961. [CrossRef]
124. Holmes, D.R.; Reddy, V.Y.; Turi, Z.G.; Doshi, S.K.; Sievert, H.; Buchbinder, M.; Mullin, C.M.; Sick, P. Percutaneous closure of the left atrial appendage versus warfarin therapy for prevention of stroke in patients with atrial fibrillation: A randomised non-inferiority trial. *Lancet* **2009**, *374*, 534–542. [CrossRef]
125. Galea, R.; De Marco, F.; Meneveau, N.; Aminian, A.; Anselme, F.; Gräni, C.; Huber, A.T.; Teiger, E.; Iriart, X.; Bosombo, F.B.; et al. Amulet or Watchman Device for Percutaneous Left Atrial Appendage Closure: Primary Results of the SWISS-APERO Randomized Clinical Trial. *Circulation* **2022**, *145*, 724–738. [CrossRef] [PubMed]
126. Prakash, R.; Saw, J. Imaging for percutaneous left atrial appendage closure. *Catheter. Cardiovasc. Interv.* **2016**, *92*, 437–450. [CrossRef]
127. Oda, S.; Honda, K.; Yoshimura, A.; Katahira, K.; Noda, K.; Oshima, S.; Yuki, H.; Kidoh, M.; Utsunomiya, D.; Nakaura, T.; et al. 256-Slice coronary computed tomographic angiography in patients with atrial fibrillation: Optimal reconstruction phase and image quality. *Eur. Radiol.* **2015**, *26*, 55–63. [CrossRef] [PubMed]

128. Martinez, M.W.; Kirsch, J.; Williamson, E.E.; Syed, I.S.; Feng, D.; Ommen, S.; Packer, D.L.; Brady, P.A. Utility of Nongated Multidetector Computed Tomography for Detection of Left Atrial Thrombus in Patients Undergoing Catheter Ablation of Atrial Fibrillation. *JACC: Cardiovasc. Imaging* **2009**, *2*, 69–76. [CrossRef]
129. Hur, J.; Kim, Y.J.; Lee, H.-J.; Nam, J.E.; Hong, Y.; Kim, H.Y.; Lee, J.W.; Choi, B.W. Cardioembolic Stroke: Dual-Energy Cardiac CT for Differentiation of Left Atrial Appendage Thrombus and Circulatory Stasis. *Radiology* **2012**, *263*, 688–695. [CrossRef]
130. Rajwani, A.; Nelson, A.J.; Shirazi, M.G.; Disney, P.J.S.; Teo, K.S.L.; Wong, D.T.L.; Young, G.D.; Worthley, S.G. CT sizing for left atrial appendage closure is associated with favourable outcomes for procedural safety. *Eur. Hear. J. Cardiovasc. Imaging* **2016**, *18*, 1361–1368. [CrossRef]
131. Wang, Y.; Di Biase, L.; Horton, R.P.; Nguyen, T.; Morhanty, P.; Natale, A. Left Atrial Appendage Studied by Computed Tomography to Help Planning for Appendage Closure Device Placement. *J. Cardiovasc. Electrophysiol.* **2010**, *21*, 973–982. [CrossRef]
132. Jaguszewski, M.; Manes, C.; Puippe, G.; Salzberg, S.; Müller, M.; Falk, V.; Lüscher, T.; Luft, A.; Alkadhi, H.; Landmesser, U. Cardiac CT and echocardiographic evaluation of peri-device flow after percutaneous left atrial appendage closure using the AMPLATZER cardiac plug device. *Catheter. Cardiovasc. Interv.* **2014**, *85*, 306–312. [CrossRef] [PubMed]
133. Clemente, A.; Avogliero, F.; Berti, S.; Paradossi, U.; Jamagidze, G.; Rezzaghi, M.; Della Latta, D.; Chiappino, D. Multimodality imaging in preoperative assessment of left atrial appendage transcatheter occlusion with the Amplatzer Cardiac Plug. *Eur. Hear. J. Cardiovasc. Imaging* **2015**, *16*, 1276–1287. [CrossRef] [PubMed]
134. Diwakar, M.; Tripathi, A.; Joshi, K.; Sharma, A.; Singh, P.; Memoria, M.; Kumar, N. A comparative review: Medical image fusion using SWT and DWT. *Mater. Today: Proc.* **2020**, *37*, 3411–3416. [CrossRef]
135. Diwakar, M.; Tripathi, A.; Joshi, K.; Memoria, M.; Singh, P.; Kumar, N. Latest trends on heart disease prediction using machine learning and image fusion. *Mater. Today: Proc.* **2020**, *37*, 3213–3218. [CrossRef]
136. Joshi, K.; Kumar, M.; Tripathi, A.; Kumar, A.; Sehgal, J.; Barthwal, A. *Latest Trends in Multi-Modality Medical Image Fusion: A Generic Review*; Springer: Singapore, 2022; Volume 434, pp. 663–671. [CrossRef]

Disclaimer/Publisher's Note: The statements, opinions and data contained in all publications are solely those of the individual author(s) and contributor(s) and not of MDPI and/or the editor(s). MDPI and/or the editor(s) disclaim responsibility for any injury to people or property resulting from any ideas, methods, instructions or products referred to in the content.